A robust and efficient numerical method to compute the dynamics of the rotating two-component dipolar Bose-Einstein condensates

Qinglin Tang[a,b], Yong Zhang[c,*], Norbert J. Mauser[d]

[a] *Institut Elie Cartan de Lorraine, Université de Lorraine, Inria Nancy-Grand Est, F-54506 Vandoeuvre-lès-Nancy Cedex, France*

[b] *Laboratoire de Mathématiques Raphaël Salem, Université de Rouen, Technopôle du Madrillet, 76801 Saint-Etienne-du-Rouvray, France*

[c] *Université de Rennes 1, IRMAR, Campus de Beaulieu, 35042 Rennes Cédex, France*

[d] *Wolfgang Pauli Institute c/o Fak. Mathematik, University Wien, Oskar-Morgenstern-Platz 1, 1090 Vienna, Austria*

Abstract

We present a robust and efficient numerical method to compute the dynamics of the rotating two-component dipolar Bose-Einstein condensates (BEC). Using the rotating Lagrangian coordinates transform [13], we reformulate the original coupled Gross-Pitaevskii equations (CGPE) into new equations where the rotating term vanishes and the potential becomes time-dependent. A time-splitting Fourier pseudospectral method is proposed to numerically solve the new equations where the nonlocal Dipole-Dipole Interactions (DDI) are computed by a newly-developed Gaussian-sum (GauSum) solver [23] which helps achieve spectral accuracy in space within $O(N \log N)$ operations (N is the total number of grid points). The new method is spectrally accurate in space and second order accurate in time - these accuracies are confirmed numerically. Dynamical properties of some physical quantities, including the total mass, energy, center of mass and angular momentum expectation, are presented and confirmed numerically. Interesting dynamical phenomena that are peculiar to the rotating two-component dipolar BECs, such as dynamics of center of mass, quantized vortex lattices dynamics and the collapse dynamics in 3D, are presented.

Keywords: two-component dipolar BEC, dynamics, Gaussian-sum method, rotating Lagrangian coordinates, time splitting, Fourier spectral method, collapse dynamics

1. Introduction

The Bose-Einstein condensation (BEC) yields most interesting state-of-the-art experiments for relatively large quantum systems and has been extensively studied since its first experimental realization in 1995 [3, 17, 21]. A subsequent achievement of quantum vortices in rotating BECs [1, 40, 25] broadens the attention to explore vortex states and their dynamics associated with superfluidity. Initially, the experiments/simulations were limited to the case of short-range interatomic interactions [43]. Recently, considerable attention has been drawn to systems with long-range dipole-dipole interactions (DDIs) in ultracold physics [33]. For heteronuclear molecules, DDIs come from their electric dipole moments [46]. In a state with a well-defined angular momentum, molecules do not have a dipole moment. Nevertheless, dipolar moments can be induced when molecules are polarized via an external electric field. For atoms, dipolar interactions arise from their magnetic moments and become significant for large electronic spin. Recent experiments on dipolar BECs of Cr atoms and others [6, 28, 39] demonstrated very well for such interactions and has spurred new impetus in the study of dipolar BECs.

*Corresponding author.

Email addresses: tqltql2010@gmail.com (Qinglin Tang), sunny5zhang@gmail.com (Yong Zhang), norbert.mauser@univie.ac.at (Norbert J. Mauser)

Due to the presence of anisotropic DDI, vortices in rotating dipolar BECs exhibit novel properties and richer phenomena [20, 35, 36, 57]. On the other hand, thanks to the development of trapping techniques, binary condensates are also realised [29, 31, 34] and provide an ideal system for studying phase transitions and coexistence of different phases [2, 27, 55]. Far from being a trivial extension of the single-component BEC, the physics of a dipolar mixture may feature different and remarkable properties, such as the domain walls, vortons and square vortex lattices [31, 34, 51].

Very recently, the vortices of rotating two-component dipolar BECs under different trapping potentials have been investigated in several studies by physicists [26, 51, 55, 56, 59]. At temperatures T much smaller than the critical temperature T_c, the properties of rotating two-component dipolar BECs are well described by the macroscopic complex-valued wave function $\Psi = (\psi_1(\mathbf{x},t), \psi_2(\mathbf{x},t))^T$ calculated from the three-dimensional (3D) Coupled Gross–Pitaevskii Equations (CGPE) with DDI term. Moreover, the 3D CGPE can be reduced to an effective two-dimensional (2D) equation if the external potential is highly anisotropic, i.e. much stronger in $z-$direction [18, 10]. In a unified way, the $d-$dimensional ($d = 2$ or 3) dimensionless CGPE with DDI term reads as [56, 51, 52, 59, 9]:

$$i\partial_t \psi_j(\mathbf{x},t) = \left[-\frac{1}{2}\nabla^2 + V_j(\mathbf{x}) - \Omega L_z + \sum_{k=1}^{2}\left(\beta_{jk}|\psi_k|^2 + \lambda_{jk}\,\Phi_k(\mathbf{x},t)\right)\right]\psi_j(\mathbf{x},t), \tag{1.1}$$

$$\Phi_j(\mathbf{x},t) = U_{\rm dip} * |\psi_j|^2, \qquad \psi_j(\mathbf{x},t=0) = \psi_j^0(\mathbf{x}), \qquad j = 1,\ 2, \quad \mathbf{x}\in\mathbb{R}^d, \quad t \geq 0. \tag{1.2}$$

Here, Φ_j is defined as a convolution of the kernel $U_{\rm dip}$ with the density $|\psi_j|^2$ where $*$ denotes the convolution operator, t denotes time, $\mathbf{x} = (x,y,z)^T \in \mathbb{R}^3$ and/or $\mathbf{x} = (x,y)^T \in \mathbb{R}^2$ is the Cartesian coordinate vector. The constant β_{jk} describes the strength of the short-range interactions in a condensate (positive/negative for repulsive/attractive interaction), $L_z = -i(x\partial_y - y\partial_x) = -i\partial_\theta$ is the z-component of the angular momentum and Ω represents the rotating frequency. $V_j(\mathbf{x})$ $(j = 1, 2)$ is a given real-valued external trapping potential determined by the type of system under investigation. In most BEC experiments, a harmonic potential is chosen to trap the condensates, i.e. for $j = 1, 2$

$$V_j(\mathbf{x}) = \frac{1}{2}\begin{cases} \gamma_{x,j}^2 x^2 + \gamma_{y,j}^2 y^2, & d = 2, \\ \gamma_{x,j}^2 x^2 + \gamma_{y,j}^2 y^2 + \gamma_{z,j}^2 z^2, & d = 3, \end{cases} \tag{1.3}$$

where $\gamma_{v,j}$ $(v = x, y, z)$ are dimensionless constants representing the trapping frequencies in v-direction. Moreover, λ_{ij} $(i, j = 1, 2)$ is a constant characterizing the strength of DDI and $U_{\rm dip}(\mathbf{x})$ is the long-range DDI potential. In 3D, $U_{\rm dip}(\mathbf{x})$ reads as

$$U_{\rm dip}(\mathbf{x}) = \frac{3}{4\pi|\mathbf{x}|^3}\left[1 - \frac{3(\mathbf{x}\cdot\mathbf{n})^2}{|\mathbf{x}|^2}\right] = -\delta(\mathbf{x}) - 3\,\partial_{\mathbf{nn}}\left(\frac{1}{4\pi|\mathbf{x}|}\right), \qquad \mathbf{x}\in\mathbb{R}^3, \tag{1.4}$$

with $\mathbf{n} = (n_1, n_2, n_3)^T$, a given unit vector i.e. $|\mathbf{n}(t)| = \sqrt{n_1^2 + n_2^2 + n_3^2} = 1$, representing the dipole axis (or dipole moment), $\partial_{\mathbf{n}} = \mathbf{n}\cdot\nabla$ and $\partial_{\mathbf{nn}} = \partial_{\mathbf{n}}(\partial_{\mathbf{n}})$. While in 2D, it is defined as [7, 18]

$$U_{\rm dip}(\mathbf{x}) = -\frac{3}{2}\left(\partial_{\mathbf{n}_\perp\mathbf{n}_\perp} - n_3^2\nabla_\perp^2\right)\left(\frac{1}{2\pi|\mathbf{x}|}\right), \qquad \mathbf{x}\in\mathbb{R}^2, \tag{1.5}$$

where $\nabla_\perp = (\partial_x, \partial_y)^T$, $\mathbf{n}_\perp = (n_1, n_2)^T$, $\partial_{\mathbf{n}_\perp} = \mathbf{n}_\perp\cdot\nabla_\perp$ and $\partial_{\mathbf{n}_\perp\mathbf{n}_\perp} = \partial_{\mathbf{n}_\perp}(\partial_{\mathbf{n}_\perp})$. In fact, for smooth densities, the DDI potential can be reformulated via the Coulomb potential whose convolution kernel is $U_{\rm cou}(\mathbf{x}) = \frac{1}{2^{d-1}|\mathbf{x}|}$. To be precise, the 3D DDI potential (1.4) is reformulated as follows

$$\Phi_j(\mathbf{x}) = -\rho_j - 3\,\partial_{\mathbf{n}}\partial_{\mathbf{n}}\left(\frac{1}{4\pi|\mathbf{x}|} * \rho_j\right) = -\rho_j - 3\,\frac{1}{4\pi|\mathbf{x}|} * (\partial_{\mathbf{n}}\partial_{\mathbf{n}}\rho_j), \quad \mathbf{x}\in\mathbb{R}^3, \tag{1.6}$$

while the 2D DDI (1.5) is rewritten as

$$\Phi_j(\mathbf{x}) = -\frac{3}{2}\,\frac{1}{2\pi|\mathbf{x}|} * [\left(\partial_{\mathbf{n}_\perp\mathbf{n}_\perp} - n_3^2\nabla_\perp^2\right)\rho_j], \quad \mathbf{x}\in\mathbb{R}^2. \tag{1.7}$$

The time dependent CGPE in (1.1)–(1.2) conserve two important quantities: the total *mass* (or *normalization*) of the wave function

$$\mathcal{N}(t) := \|\Psi(\mathbf{x},t)\|^2 = \mathcal{N}_1(t) + \mathcal{N}_2(t) \equiv \|\Psi(\mathbf{x},0)\|^2 = 1, \tag{1.8}$$

where $\mathcal{N}_j(t)$ is the mass of the jth component at time $t \geq 0$, which reads as

$$\mathcal{N}_j(t) := \int_{\mathbb{R}^d} |\psi_j(\mathbf{x},t)|^2 d\mathbf{x} \equiv \mathcal{N}_j(0), \quad j = 1,2,\ t \geq 0, \tag{1.9}$$

and the *energy per particle*

$$\begin{aligned} \mathcal{E}(\Psi(\mathbf{x},t)) &= \int_{\mathbb{R}^d} \Bigg[\sum_{j=1}^{2} \left(\frac{1}{2}|\nabla\psi_j|^2 + V_j(\mathbf{x})|\psi_j|^2 + \frac{\beta_{jj}}{2}|\psi_j|^4 + \frac{\lambda_{jj}}{2}\Phi_j\,|\psi_j|^2 - \Omega\psi_j^* L_z\psi_j \right) \\ &\qquad + \frac{1}{2}(\beta_{12}+\beta_{21})|\psi_1|^2|\psi_2|^2 + \frac{1}{4}\,(\lambda_{12}+\lambda_{21})(\Phi_1|\psi_2|^2 + \Phi_2|\psi_1|^2) \Bigg] d\mathbf{x} \\ &\equiv \mathcal{E}(\Psi(\mathbf{x},0)), \qquad\qquad t \geq 0. \end{aligned} \tag{1.10}$$

There have been extensive mathematical and numerical studies on the single-component dipolar BEC; we refer the reader to [7, 9, 10, 14, 15, 19, 30, 53, 54]. For the rotating two-component BEC without DDI, dynamics and stationary states have been studied in [58, 50] and [49, 48, 38], respectively. Recently, there is growing interest from physicists for studying the properties of (non)-rotating two-component BEC with DDI [2, 26, 27, 44, 51, 52, 55, 56, 59]. However, up to now, there are few numerical studies on the rotating two-component BEC with DDI based on the CGPE (1.1)–(1.2). In this paper, we give an exhaustive mathematical study of new efficient numerical methods of the rotating two-component dipolar BECs.

To compute the dynamics, the main difficulties lie in the nonlocal DDI evaluation and proper treatment of the rotation term. As is shown before, the DDI can be computed via the Coulomb potential. On bounded rectangular domains with Dirichlet boundary conditions, the Discrete Sine Transform (DST) method applies directly [9, 10]. However, the DST method requires a quite large computation domain in order to achieve a satisfactory accuracy. In 2014, Jiang *et al.* [32] proposed a NonUniform Fast Fourier Transform (NUFFT) solver by adopting the polar/spherical coordinates in the Fourier domain, we refer to [12, 14] for extensions and applications in the context of Nolinear Schrödinger equation (NLSE). Recently, using an accurate Gaussian-summation approximation of the convolution kernel, Zhang *et al.* [23] introduced an even more efficient and accurate method, which we shall refer to as GauSum solver hereafter. Both NUFFT and GauSum solver are fast algorithms with a complexity of $O(N \log N)$ where N is the total number of grid points. Compared with the NUFFT solver, the GauSum solver is 3-5 times faster, thus it is the state-of-the-art method for applications [5]. For the rotation term, Bao *et al.* [13] developed a rotating Lagrangian coordinates transformation method to reformulate the rotating term into a time-dependent trapping potential, and this method allows for the implementation of high order time marching schemes [4, 16, 41]. Note that in Eulerian coordinates, additional efforts have to be made for the rotational term. In the literature, to discretise the rotational term, popular approaches either introduce ADI technique or use polar/spherical coordinate. The former method introduces extra splitting error and is complicated to be extended to higher order time marching schemes, while the later imposes artificial boundary at the origin point $r = 0$ and the radial direction is discretised by lower order schemes, for example finite difference method (FDM) and finite element method (FEM).

The main objectives of this paper are threefold.

Using the rotating Lagrangian coordinates transform [13], we reformulate the original CGPE into new equations without rotating term. Then we develop a robust and efficient numerical method to compute dynamics of the new equations by incorporating the GauSum solver [23], which is designed to compute the nonlocal DDI, into an adapted version of the time-splitting Fourier pseudospectral method. Detailed numerical results are presented that confirm the spectral accuracy in space and second order temporal accuracy of the proposed method in 2D and 3D respectively. Develop the

dynamical laws for the mass and energy, the angular momentum expectation and center of mass, together with some proofs. An analytical solution with special initial data is also presented. Apply our method to study the dynamics of center of mass, quantized vortex lattices and non-rotating dipolar BECs in different setups. In particular, phase separation and collapse dynamics are observed numerically for the 3D cases.

The rest of the paper is organized as follows: In Section 2, we present a brief review of the Gaussian-sum method. In Section 3, we derive some dynamical laws for some physical quantities that are usually considered for the standard GPE. We then propose an efficient and robust time splitting Fourier pseudospectral numerical method for simulating the dynamics. Detailed convergence tests are presented in Section 4 to confirm the spatial and temporal convergence of our method, and some interesting numerical results are also reported. Finally, conclusions are drawn in Section 5.

2. The DDI evaluation by Gaussian-sum method

Due to the confining potential $V(\mathbf{x})$ in the CGPE (1.1)–(1.2), the density $\rho(\mathbf{x}) := |\psi(\mathbf{x})|^2$ is usually smooth and decays exponentially fast. As is shown by (1.6) and (1.7), the DDI computation boils down to Coulomb potential evaluation. Therefore, in this section, we shall only give a brief self-contained review of the GauSum method [23] for Coulomb potential. All subscripts in the section are omitted for brevity.

For numerical calculations we have to truncate the whole space to a bounded domain with boundary conditions(BC), e.g. a square box $\mathbf{B}_L := [-L, L]^d$ with homogeneous Dirichlet BC, then we rescale to a unit box $\mathbf{B}_1$ by setting the density ρ to be zero outside $\mathbf{B}_1$. Using a smooth approximation of $U_{\rm cou}$ (see $U_{\rm GS}$ in (2.5)), the Coulomb potential is split into two integrals, i.e. the *long-range regular integral* $I_1(\mathbf{x})$ and the *short-range singular integral* $I_2(\mathbf{x})$. To be precise,

$$\begin{aligned}
\Phi(\mathbf{x}) &\approx \int_{\mathbf{B}_1} U_{\rm cou}(\mathbf{x}-\mathbf{y})\,\rho(\mathbf{y})d\mathbf{y} = \int_{\mathbf{B}_2} U_{\rm cou}(\mathbf{y})\,\rho(\mathbf{x}-\mathbf{y})d\mathbf{y} && (2.1)\\
&= \int_{\mathbf{B}_2} U_{\rm GS}(\mathbf{y})\,\rho(\mathbf{x}-\mathbf{y})d\mathbf{y} + \int_{\mathcal{B}_\delta} \big(U_{\rm cou}(\mathbf{y}) - U_{\rm GS}(\mathbf{y})\big)\,\rho(\mathbf{x}-\mathbf{y})d\mathbf{y} + I_\delta && (2.2)\\
&:= I_1(\mathbf{x}) + I_2(\mathbf{x}) + I_\delta, \qquad \mathbf{x}\in\mathbf{B}_1. && (2.3)
\end{aligned}$$

The remainder integral I_δ is given explicitly as

$$I_\delta = \int_{\mathbf{B}_2\setminus\mathcal{B}_\delta} \big(U_{\rm cou}(\mathbf{y}) - U_{GS}(\mathbf{y})\big)\,\rho(\mathbf{x}-\mathbf{y})d\mathbf{y}, \tag{2.4}$$

where $\mathcal{B}_\delta := \{\mathbf{x}\big||\mathbf{x}|\le\delta\}$ is a very small ball centered at the origin and

$$U_{\rm GS}(\mathbf{y}) = U_{\rm GS}(|\mathbf{y}|) := \sum_{q=0}^{Q} w_q\, e^{-\tau_q^2|\mathbf{y}|^2}, \quad Q\in\mathbb{N}^+, \tag{2.5}$$

where w_q, τ_q are weights and nodes. Here, $U_{\rm GS}$ is a very accurate approximation of $U_{\rm cou}$ in the interval $[\delta, 2]$, i.e.

$$\|U_{\rm cou}(r) - U_{\rm GS}(r)\|_{L^\infty([\delta,2])} \le \varepsilon_0, \tag{2.6}$$

where ε_0 is the approximation error in L^∞ norm. For the remainder integral, we have $|I_\delta| \le C\varepsilon_0\,\delta^d\,\|\rho\|_{L^\infty}$, thus I_δ is negligible for small ε_0 and δ. Therefore, it suffices to approximate the Coulomb potential by $\Phi(\mathbf{x}) \approx I_1(\mathbf{x}) + I_2(\mathbf{x})$. We refer to [23] for more details.

To compute the *regular integral* I_1, plugging $U_{\rm GS}$ (2.5), we have

$$I_1(\mathbf{x}) = \sum_{q=0}^{Q} w_q \int_{\mathbf{B}_2} e^{-\tau_q^2|\mathbf{y}|^2}\rho(\mathbf{x}-\mathbf{y})d\mathbf{y}, \qquad \mathbf{x}\in\mathbf{B}_1. \tag{2.7}$$

The density $\rho(\mathbf{x}-\mathbf{y}), \mathbf{x}\in\mathbf{B}_1, \mathbf{y}\in\mathbf{B}_2$ is well approximated by Fourier series as follows

$$\rho(\mathbf{z}) \approx \sum_{\mathbf{k}} \widehat{\rho}_{\mathbf{k}} \prod_{j=1}^{d} e^{\frac{2\pi i\ k_j}{6}(z^{(j)}+3)}, \qquad \mathbf{z}=(z^{(1)},\ldots,z^{(d)})\in\mathbf{B}_3. \tag{2.8}$$

For the Fourier coefficients $\widehat{\rho}_{\mathbf{k}}$, we have

$$\widehat{\rho}_{\mathbf{k}} = \frac{1}{|\mathbf{B}_3|}\int_{\mathbf{B}_3} \rho(\mathbf{z}) \prod_{j=1}^{d} e^{\frac{-2\pi i\ \ k_j}{6}(z^{(j)}+3)} d\mathbf{z}, \tag{2.9}$$

where $|\mathbf{B}_3| = \prod_{j=1}^{d}(b_j-a_j)$ is the volume.

Careful calculations leads to

$$I_1(\mathbf{x}) \quad = \quad \sum_{\mathbf{k}} \widehat{\rho}_{\mathbf{k}} \left(\sum_{q=0}^{Q} w_q G_{\mathbf{k}}^q\right) \prod_{j=1}^{d} e^{\frac{2\pi i\ \ k_j}{b_j-a_j}(x^{(j)}-a_j)}, \tag{2.10}$$

where

$$G_{\mathbf{k}}^q \quad = \quad \prod_{j=1}^{d} \int_{-2}^{2} e^{-\tau_q^2|y^{(j)}|^2}\, e^{\frac{-2\pi i k_j\ y^{(j)}}{b_j-a_j}} dy^{(j)}, \tag{2.11}$$

can be pre-computed once for all if the computation grid remains unchanged.

For the *near-field correction integral* I_2, the density function $\rho_{\mathbf{x}}(\mathbf{y}) := \rho(\mathbf{x}-\mathbf{y})$ is approximated by a low-order Taylor expansion within $\mathcal{B}_\delta$ as follows

$$\rho_{\mathbf{x}}(\mathbf{y}) \approx \mathrm{P}_{\mathbf{x}}(\mathbf{y}) = \rho_{\mathbf{x}}(\mathbf{0}) + \sum_{j=1}^{d} \frac{\partial \rho_{\mathbf{x}}(\mathbf{0})}{\partial y_j} y_j + \frac{1}{2}\sum_{j,k=1}^{d} \frac{\partial^2 \rho_{\mathbf{x}}(\mathbf{0})}{\partial y_j \partial y_k} y_j\, y_k + \frac{1}{6}\sum_{j,k,\ell=1}^{d} \frac{\partial^3 \rho_{\mathbf{x}}(\mathbf{0})}{\partial y_j \partial y_k \partial y_\ell} y_j\, y_k\, y_\ell. \tag{2.12}$$

We then integrate it in spherical/polar coordinates. The computation boils down to a multiplication of the Laplacian $\Delta\rho$ since the contributions of the odd derivatives in (2.12) and off-diagonal components of the Hessian vanish. Derivatives of ρ are computed via its Fourier series. For more details, we refer the reader to [5, 23].

The GauSum method achieves a spectral accuracy and is as efficient as FFT algorithms within $O(N\log N)$ arithmetic operations [23]. The algorithm has been implemented for DDI [23] and applied in the studies of fractional Schrödinger equations [5].

3. Properties of the dynamics and the numerical method

In this section, we first present conservation laws for some commonly used quantities analogous to the rotating CGPE without DDI. Then, we extend the rotating Lagrangian coordinate transform proposed for the GPE without DDI in [13]. In the rotating Lagrangian coordinates, the rotation term vanishes, instead the potential becomes time-dependent. For the new equation, we shall propose a time-splitting Fourier spectral method incorporated with the GauSum solver to compute the dynamics.

3.1. Properties of the dynamics

Here we study the dynamical properties of the mass, energy, angular momentum expectation and center of mass. The dynamical laws can be used as benchmarks to test the numerical methods and are briefly listed here. For details, one can prove in an analogous way to the one component [47, 13] or two-component without DDI [9].

Mass and energy. The CGPE (1.1)-(1.2) conserves the mass (1.9) and energy (1.10), i.e.

$$\mathcal{N}_1(t)=\mathcal{N}_1(t=0),\quad \mathcal{N}_2(t)=\mathcal{N}_2(t=0),\quad \mathcal{N}(t):=(\mathcal{N}_1+\mathcal{N}_2)(t)=\mathcal{N}(t=0),\quad \mathcal{E}(t)=\mathcal{E}(t=0). \tag{3.1}$$

Angular momentum expectation. The *angular momentum expectation* for each component and the total angular momentum are defined respectively as

$$\langle L_z\rangle_j(t)=\int_{\mathbb{R}^d}\psi_j^*(\mathbf{x},t)L_z\psi_j(\mathbf{x},t)\,d\mathbf{x},\quad j=1,2,\quad \langle L_z\rangle(t)=\langle L_z\rangle_1(t)+\langle L_z\rangle_2(t),\quad t\geq 0. \tag{3.2}$$

Lemma 3.1. *If $V_j(\mathbf{x})$ reads as the harmonic potential, we have for $j=1,2$ and $k_j=3-j$*

$$\frac{d}{dt}\langle L_z\rangle_j(t)=w_j^-\int_{\mathbb{R}^d}xy|\psi_j|^2d\mathbf{x}+\int_{\mathbb{R}^d}|\psi_j|^2(y\partial_x-x\partial_y)\Big(\beta_{jk_j}|\psi_{k_j}|^2+\sum_{k=1}^{2}\lambda_{jk}\Phi_k(\mathbf{x},t)\Big)d\mathbf{x}, \tag{3.3}$$

Moreover, if additionally $\beta_{12}=\beta_{21}$, we have

$$\frac{d}{dt}\langle L_z\rangle(t)=\sum_{j=1}^{2}w_j^-\int_{\mathbb{R}^d}xy|\psi_j|^2d\mathbf{x}+\sum_{j,k=1}^{2}\lambda_{jk}\int_{\mathbb{R}^d}|\psi_j|^2(y\partial_x-x\partial_y)\Phi_k(\mathbf{x},t)d\mathbf{x}. \tag{3.4}$$

Here $w_j^-=\gamma_{x,j}^2-\gamma_{y,j}^2$. This implies that the total angular momentum expectation $\langle L_z\rangle(t)$ is conserved, i.e.

$$\langle L_z\rangle(t)=\langle L_z\rangle(0),\qquad t\geq 0, \tag{3.5}$$

if $\gamma_{x,j}=\gamma_{y,j}$ and one of the following condition holds: (i). $\lambda_{11}=\lambda_{12}=\lambda_{21}=\lambda_{22}=0$. (ii). $\lambda_{12}=\lambda_{21}$ and the dipole axises parallel to the z-axis, i.e. $\mathbf{n}_1=\mathbf{n}_2=(0,0,1)^T$. Moreover, the angular momentum expectation for each component is also conserved, i.e.

$$\langle L_z\rangle_j(t)=\langle L_z\rangle_j(0),\qquad j=1,2,\quad t\geq 0, \tag{3.6}$$

if additionally provided $\lambda_{12}=\lambda_{21}=\beta_{12}=\beta_{21}=0$.

Proof 3.1. *Let us take a close look at the DDI term in (3.4). Using the Plancherel's formula, we have*

$$\begin{aligned}\langle\rho_j,(y\partial_x-x\partial_y)\Phi_k\rangle &:= \int_{\mathbb{R}^d}|\psi_j|^2(-\partial_\theta\Phi_k)d\mathbf{x}=\frac{1}{(2\pi)^d}\langle\widehat{\rho}_j,\widehat{-\partial_\theta\Phi_k}\rangle &(3.7)\\ &= \frac{1}{(2\pi)^d}\langle\widehat{\rho}_j,-\partial_{\theta_\xi}\widehat{U_{\rm dip}}\widehat{\rho_k}\rangle &(3.8)\end{aligned}$$

where the Fourier transform is defined as $\widehat{f}(\xi)=\int_{\mathbb{R}^d}f(\mathbf{x})e^{-i\xi\cdot\mathbf{x}}d\mathbf{x}$,

$$\widehat{U}_{\rm dip}(\xi)=\begin{cases}-1+\frac{3(\mathbf{n}\cdot\xi)^2}{|\xi|^2}, & d=3,\\ \frac{2[(\mathbf{n}_\perp\cdot\xi)^2-n_3^2|\xi|^2]}{2|\xi|}, & d=2,\end{cases} \tag{3.9}$$

and θ,θ_ξ are the azimuth angle in physical/Fourier space respectively. For $\mathbf{n}=(0,0,1)^T$, it is easy to see that $\widehat{U}_{\rm dip}(\xi)$ is cylindrical/polar symmetric in 3D and 2D respectively, and we have

$$\begin{aligned}\langle\rho_j,-\partial_\theta\Phi_k\rangle &= \frac{1}{(2\pi)^d}\langle\widehat{\rho}_j,-\partial_{\theta_\xi}(\widehat{U_{\rm dip}}\widehat{\rho_k})\rangle=\frac{1}{(2\pi)^d}\langle\widehat{U_{\rm dip}}\widehat{\rho}_j,-\partial_{\theta_\xi}\widehat{\rho_k}\rangle &(3.10)\\ &= \langle\Phi_j,-\partial_\theta\rho_k\rangle=\langle\partial_\theta\Phi_j,\rho_k\rangle &(3.11)\\ &= -\langle\rho_k,-\partial_\theta\Phi_j\rangle. &(3.12)\end{aligned}$$

The proof is then completed due to the above anti-symmetric property in the index (j,k).

Center of mass. The total center of mass is defined as

$$\mathbf{x}_c(t) = \int_{\mathbb{R}^d} \mathbf{x}\,|\Psi(\mathbf{x},t)|^2 d\mathbf{x} =: \mathbf{x}_{c,1}(t) + \mathbf{x}_{c,2}(t), \quad t \geq 0, \tag{3.13}$$

where $\mathbf{x}_{c,j}(t)$ is defined as the (scaled) center of mass of the jth component and reads as follows

$$\mathbf{x}_{c,j}(t) = \int_{\mathbb{R}^d} \mathbf{x}\,|\psi_j(\mathbf{x},t)|^2 d\mathbf{x}, \quad j = 1,\ 2, \quad t \geq 0. \tag{3.14}$$

Lemma 3.2. *If $V_j(\mathbf{x})$ reads as the harmonic potential, we have for $j = 1, 2$ and $k_j = 3 - j$*

$$\ddot{\mathbf{x}}_{c,j} - 2\Omega J_d \dot{\mathbf{x}}_{c,j} + (\Lambda_{d,j} + \Omega^2 J_d^2)\mathbf{x}_{c,j} = \int_{\mathbb{R}^d} \Big(\beta_{j,k_j}|\psi_{k_j}|^2 + \lambda_{j,k_j}\Phi_{k_j}\Big)\nabla|\psi_j|^2\, d\mathbf{x}, \tag{3.15}$$

$$\mathbf{x}_{c,j}^0 = \int_{\mathbb{R}^d} \mathbf{x}\,|\psi_j^0(\mathbf{x})|^2 d\mathbf{x}, \qquad \dot{\mathbf{x}}_{c,j}^0 = \int_{\mathbb{R}^d} \mathrm{Im}(\bar{\psi}_j^0 \nabla \psi_j^0) d\mathbf{x} + \Omega J_d \mathbf{x}_{c,j}^0, \tag{3.16}$$

where,

$$J_d = \begin{cases} \begin{pmatrix} 0 & 1 \\ -1 & 0 \end{pmatrix}, \\ \begin{pmatrix} J_2 & \mathbf{0} \\ \mathbf{0} & \mathbf{0} \end{pmatrix}, \end{cases} \qquad \Lambda_{d,j} = \begin{cases} \begin{pmatrix} \gamma_{x,j}^2 & 0 \\ 0 & \gamma_{y,j}^2 \end{pmatrix}, & d = 2, \\ \begin{pmatrix} \Lambda_{j,2} & \mathbf{0} \\ \mathbf{0} & \gamma_{z,j}^2 \end{pmatrix}, & d = 3. \end{cases} \tag{3.17}$$

Moreover, if $V_1(\mathbf{x}) = V_2(\mathbf{x})$, $\beta_{12} = \beta_{21}$ and $\lambda_{12} = \lambda_{21}$, we have

$$\ddot{\mathbf{x}}_c - 2\Omega J_d \dot{\mathbf{x}}_c + (\Lambda_{d,1} + \Omega^2 J_d^2)\mathbf{x}_c = \mathbf{0}, \tag{3.18}$$

$$\mathbf{x}_c^0 = \mathbf{x}_{c,1}^0 + \mathbf{x}_{c,2}^0, \qquad \dot{\mathbf{x}}_c^0 = \dot{\mathbf{x}}_{c,1}^0 + \dot{\mathbf{x}}_{c,2}^0. \tag{3.19}$$

An analytical solution for special initial data. An interesting application of the dynamic law (3.18) for the total center of mass is that under some circumstances we can construct an analytical solution to the CGPE. Precisely speaking, suppose the initial condition ψ_j^0 in (1.2) is chosen as

$$\psi_j^0(\mathbf{x}) = \phi_j^s(\mathbf{x} - \mathbf{x}_0), \qquad \mathbf{x} \in \mathbb{R}^d, \tag{3.20}$$

where $\mathbf{x}_0 \in \mathbb{R}^d$ is a given point and ϕ_j^s $(j = 1, 2)$ is a stationary state of the CGPE, i.e.

$$\mu_j^s \phi_j^s = \left[-\frac{1}{2}\nabla^2 + V_j(\mathbf{x}) - \Omega L_z + \sum_{k=1}^{2}\left(\beta_{jk}|\phi_k^s|^2 + \lambda_{jk} U_{\mathrm{dip}} * |\phi_k^s|^2\right)\right]\phi_j^s, \tag{3.21}$$

$$\int_{\mathbb{R}^d} |\phi_j^s|^2\, d\mathbf{x} = 1, \quad j = 1, 2. \tag{3.22}$$

where $\mu_j^s \in \mathbb{R}$ $(j = 1, 2)$ are the chemical potentials. With this initial value, and suppose $V_1(\mathbf{x}) = V_2(\mathbf{x})$, the exact solution of the CGPE with harmonic potential can be constructed as

$$\psi_j(\mathbf{x},t) = \phi_j^s(\mathbf{x} - \mathbf{x}_c(t))e^{-i\mu_j^s t} e^{iw(\mathbf{x},t)}, \quad \mathbf{x} \in \mathbb{R}^d, \quad t \geq 0, \tag{3.23}$$

where $w(\mathbf{x},t)$ is linear in $\mathbf{x}$, i.e.

$$w(\mathbf{x},t) = \mathbf{c}_1(t) \cdot \mathbf{x} + \mathbf{c}_2(t), \quad \mathbf{x} \in \mathbb{R}^d, \quad t \geq 0, \tag{3.24}$$

with some functions $\mathbf{c}_1(t)$, $\mathbf{c}_2(t)$, and $\mathbf{x}(t)$ satisfying the ODE (3.18) with initial condition

$$\mathbf{x}_c^0 = \mathbf{x}^0, \qquad \dot{\mathbf{x}}_c^0 = -\Omega J_d \mathbf{x}^0. \tag{3.25}$$

3.2. Numerical method

3.2.1. CGPE under rotating Lagrangian coordinates

In this section, we first introduce a rotating Lagrangian coordinate and then reformulate the CGPE (1.1)–(1.2) in the new coordinate system. For any time $t \geq 0$, let $\mathbf{A}_d(t)$ be an orthogonal rotational matrix in $\mathbb{R}^d$ defined as [13, 41]

$$\mathbf{A}_d(t) = \begin{pmatrix} \cos(\Omega t) & \sin(\Omega t) \\ -\sin(\Omega t) & \cos(\Omega t) \end{pmatrix}, \quad \text{if } d = 2, \qquad \mathbf{A}_d(t) = \begin{pmatrix} \mathbf{A}_2(t) & \mathbf{0} \\ \mathbf{0} & 1 \end{pmatrix}, \quad \text{if } d = 3. \tag{3.26}$$

It is easy to verify that $\mathbf{A}_d^{-1}(t) = \mathbf{A}_d^T(t)$ for any $t \geq 0$ and $A(0) = I$ with I the identity matrix. For $\forall\ t \geq 0$, the *rotating Lagrangian coordinates* $\widetilde{\mathbf{x}}$ is defined as

$$\widetilde{\mathbf{x}} = \mathbf{A}_d^{-1}(t)\mathbf{x} = \mathbf{A}_d^T(t)\mathbf{x} \quad \Longleftrightarrow \quad \mathbf{x} = \mathbf{A}_d(t)\widetilde{\mathbf{x}}, \quad \mathbf{x} \in \mathbb{R}^d, \quad t \geq 0. \tag{3.27}$$

Denotes the wave function in the new coordinates as $\phi_j(\widetilde{\mathbf{x}}, t)$:

$$\phi_j(\widetilde{\mathbf{x}}, t) := \psi_j(\mathbf{x}, t) = \psi_j\left(\mathbf{A}_d(t)\widetilde{\mathbf{x}}, t\right), \quad j = 1, 2 \qquad \widetilde{\mathbf{x}} \in \mathbb{R}^d, \quad t \geq 0. \tag{3.28}$$

By simple calculation, we have

$$\begin{aligned} &i\partial_t \phi_j(\widetilde{\mathbf{x}}, t) = i\partial_t \psi_j(\mathbf{x}, t) + i\nabla_{\mathbf{x}}\psi_j(\mathbf{x}, t) \cdot \left(\dot{\mathbf{A}}_d(t)\widetilde{\mathbf{x}}\right) = i\partial_t \psi_j(\mathbf{x}, t) + \Omega L_z \psi_j(\mathbf{x}, t), \\ &\nabla_{\widetilde{\mathbf{x}}}\phi_j(\widetilde{\mathbf{x}}, t) = A_d^{-1}(t)\nabla_{\mathbf{x}}\psi_j(\mathbf{x}, t), \quad \nabla_{\widetilde{\mathbf{x}}}^2\phi_j(\widetilde{\mathbf{x}}, t) = \nabla_{\mathbf{x}}^2\psi_j(\mathbf{x}, t), \quad \mathbf{x} \in \mathbb{R}^d, \quad t \geq 0. \end{aligned}$$

Substituting the above derivatives into (1.1)-(1.2) leads to the following d-dimensional CGPE in the rotating Lagrangian coordinates $\widetilde{\mathbf{x}}$, for $j = 1, 2$

$$i\frac{\partial \phi_j(\widetilde{\mathbf{x}}, t)}{\partial t} = \left[-\frac{1}{2}\nabla^2 + \mathcal{W}_j(\widetilde{\mathbf{x}}, t) + \sum_{k=1}^{2}\left(\beta_{jk}|\phi_k|^2 + \lambda_{jk}\widetilde{\Phi}_k\right)\right]\phi_j, \quad \widetilde{\mathbf{x}} \in \mathbb{R}^d, \quad t > 0, \tag{3.29}$$

$$\widetilde{\Phi}_k(\widetilde{\mathbf{x}}, t) = \widetilde{U}_{\rm dip} * |\phi_k|^2, \qquad \phi_j(\widetilde{\mathbf{x}}, 0) := \phi_j^0(\widetilde{\mathbf{x}}) = \psi_j^0(\mathbf{x}), \qquad \widetilde{\mathbf{x}} = \mathbf{x} \in \mathbb{R}^d. \tag{3.30}$$

Here, $\mathcal{W}_j(\widetilde{\mathbf{x}}, t) = V_j(\mathbf{A}_d(t)\widetilde{\mathbf{x}})$ $(j = 1, 2)$ and the DDI kernel $\widetilde{U}_{\rm dip}(\widetilde{\mathbf{x}}, t)$ reads as

$$\widetilde{U}_{\rm dip}(\widetilde{\mathbf{x}}, t) = \begin{cases} -\delta(\widetilde{\mathbf{x}}) - 3\,\partial_{\mathbf{m}(t)\mathbf{m}(t)}\left(\frac{1}{4\pi|\widetilde{\mathbf{x}}|}\right), & d = 3, \\ -\frac{3}{2}\left(\partial_{\mathbf{m}_\perp(t)\mathbf{m}_\perp(t)} - m_3^2\ \nabla_\perp^2\right)\left(\frac{1}{2\pi|\widetilde{\mathbf{x}}|}\right), & d = 2, \end{cases} \tag{3.31}$$

with $\mathbf{m}(t) \in \mathbb{R}^3$ defined as $\mathbf{m}(t) = \mathbf{A}_d^{-1}(t)\mathbf{n} = \big(m_1(t), m_2(t), m_3(t)\big)^T$ and $\mathbf{m}_\perp(t) := \big(m_1(t), m_2(t)\big)^T$.

In rotating Lagrangian coordinates, the energy associated with the CGPE (3.29)–(3.30) is defined as

$$\begin{aligned} \widetilde{\mathcal{E}}(t) \quad &= \quad \sum_{j=1}^{2}\int_{\mathbb{R}^d}\left[\frac{1}{2}|\nabla\phi_j|^2 + W_j(\widetilde{\mathbf{x}}, t)|\phi_j|^2 + \sum_{k=1}^{2}\left(\frac{\beta_{jk}}{2}|\phi_k|^2 + \frac{\lambda_{jk}}{2}\Phi_k\right)|\phi_j|^2\right]d\widetilde{\mathbf{x}} \\ &\quad -\sum_{j=1}^{2}\int_{\mathbb{R}^d}\int_0^t\left[\partial_\tau \mathcal{W}_j(\widetilde{\mathbf{x}}, \tau)d\tau + \sum_{k=1}^{2}\frac{\lambda_{jk}}{2}(\partial_\tau \widetilde{U}_{\rm dip}) * |\phi_k|^2\right]|\phi_j|^2 d\widetilde{\mathbf{x}} \\ &=: \quad \widetilde{\mathcal{E}}_{\rm kin}(t) + \widetilde{\mathcal{E}}_{\rm pot}(t) + \widetilde{\mathcal{E}}_{\rm short}(t) + \widetilde{\mathcal{E}}_{\rm dip}(t) + \widetilde{\mathcal{E}}_{\rm extra}(t), \end{aligned} \tag{3.32}$$

where

$$\widetilde{\mathcal{E}}_{\rm kin}(t) = \frac{1}{2}\int_{\mathbb{R}^d}\Big[|\nabla\phi_1|^2 + |\nabla\phi_2|^2\Big]d\widetilde{\mathbf{x}}, \qquad \widetilde{\mathcal{E}}_{\rm pot}(t) = \int_{\mathbb{R}^d}\Big[W_1(\widetilde{\mathbf{x}}, t)|\phi_1|^2 + W_2(\widetilde{\mathbf{x}}, t)|\phi_2|^2\Big]d\widetilde{\mathbf{x}},$$

$$\widetilde{\mathcal{E}}_{\rm short}(t) = \frac{1}{2}\sum_{j,k=1}^{2}\beta_{jk}\int_{\mathbb{R}^d}|\phi_j|^2|\phi_k|^2 d\widetilde{\mathbf{x}}, \quad \widetilde{\mathcal{E}}_{\rm dip}(t) = \frac{1}{2}\sum_{j,k=1}^{2}\lambda_{jk}\int_{\mathbb{R}^d}\Phi_k|\phi_j|^2 d\widetilde{\mathbf{x}},$$

$$\widetilde{\mathcal{E}}_{\rm extra}(t) = -\sum_{j=1}^{2}\int_{\mathbb{R}^d}\int_0^t\left[\partial_\tau \mathcal{W}_j(\widetilde{\mathbf{x}}, \tau)d\tau + \sum_{k=1}^{2}\frac{\lambda_{jk}}{2}(\partial_\tau \widetilde{U}_{\rm dip}) * |\phi_k|^2\right]|\phi_j|^2 d\widetilde{\mathbf{x}},$$

and

$$\partial_t \widetilde{U}_{\rm dip}(\widetilde{\mathbf{x}},t) = -3 \begin{cases} 2\,\partial_{\dot{\mathbf{m}}(t)\mathbf{m}(t)} \left(\frac{1}{4\pi|\widetilde{\mathbf{x}}|}\right), & d=3, \\ \partial_{\dot{\mathbf{m}}_\perp(t)\mathbf{m}_\perp(t)} \left(\frac{1}{2\pi|\widetilde{\mathbf{x}}|}\right), & d=2. \end{cases} \tag{3.33}$$

Remark 3.1. *If $V_j(\mathbf{x})$ is a harmonic potential as defined in (1.3), then $W_j(\widetilde{\mathbf{x}},t)$ has the form*

$$\mathcal{W}_j(\widetilde{\mathbf{x}},t) = \frac{w_j^+}{4}(\widetilde{x}^2+\widetilde{y}^2) + \frac{w_j^-}{4}\left[(\widetilde{x}^2-\widetilde{y}^2)\cos(2\Omega t) + 2\widetilde{x}\widetilde{y}\sin(2\Omega t)\right] + \begin{cases} 0 & d=2, \\ \frac{1}{2}\gamma_{z,j}^2\widetilde{z}^2, & d=3, \end{cases} \tag{3.34}$$

where $w_j^+ = \gamma_{x,j}^2+\gamma_{y,j}^2$ and $w_j^- = \gamma_{x,j}^2-\gamma_{y,j}^2$. Therefore, when the external potential is either a box-potential or a harmonic potential which is radially symmetric in two dimensions (2D) or cylindrically symmetric in three dimensions (3D), i.e. $\gamma_{x,j}=\gamma_{y,j}:=\gamma_{r,j}$, the potential $W_j(\widetilde{\mathbf{x}},t)$ becomes time-independent.

Compared to (1.1)–(1.2), the rotating term now vanishes in the new CGPE (3.29)–(3.30). Instead, the trapping potential and DDI kernel now become time-dependent. The absence of rotating term now allows us to develop an efficient method to solve (3.29)–(3.30).

3.2.2. Time splitting Fourier pseudospectral method

Here we shall consider the new equation (3.29)–(3.30). Due to the trapping potential, the wave functions decay exponentially. Therefore it suffices to truncate the problem into a sufficiently large bounded computational domain $\mathcal{D}=[a,b]\times[c,e]\times[f,g]$ if $d=3$, or $\mathcal{D}=[a,b]\times[c,e]$ if $d=2$. From $t=t_n$ to $t=t_{n+1}:=t_n+\Delta t$, the CGPE will be solved in two steps, i.e. for $j=1,2$ one first solves

$$i\partial_t\phi_j(\widetilde{\mathbf{x}},t) = -\frac{1}{2}\nabla^2\phi_j(\widetilde{\mathbf{x}},t), \quad \widetilde{\mathbf{x}}\in\mathcal{D}, \quad t_n\le t\le t_{n+1}, \tag{3.35}$$

with periodic boundary conditions on the boundary $\partial\mathcal{D}$ for a time step of length Δt, then solves

$$i\frac{\partial\phi_j(\widetilde{\mathbf{x}},t)}{\partial t} = \left[\mathcal{W}_j(\widetilde{\mathbf{x}},t) + \sum_{k=1}^{2}\left(\beta_{jk}|\phi_k|^2 + \lambda_{jk}\widetilde{\Phi}_k\right)\right]\phi_j \qquad \widetilde{\mathbf{x}}\in\mathcal{D}, \quad t_n\le t\le t_{n+1}, \tag{3.36}$$

$$\widetilde{\Phi}_k(\widetilde{\mathbf{x}},t) = \left(\widetilde{U}_{\rm dip} * \widetilde{\rho}_k\right)(\widetilde{\mathbf{x}},t), \qquad k=1,2, \qquad \widetilde{\mathbf{x}}\in\mathcal{D}, \quad t_n\le t\le t_{n+1}, \tag{3.37}$$

for the same time step. Here, $\widetilde{\rho}_k(\widetilde{\mathbf{x}},t)=|\phi_k(\widetilde{\mathbf{x}},t)|^2$ if $\widetilde{\mathbf{x}}\in\mathcal{D}$ and $\widetilde{\rho}_k(\widetilde{\mathbf{x}},t)=0$ otherwise. The linear subproblem (3.35) will be discretised in space by the Fourier pseudospectral method and integrated in time exactly in the phase space, while the nonlinear subproblem (3.36)-(3.37) preserves the density point-wisely, i.e. $|\phi_j(\widetilde{\mathbf{x}},t)|^2\equiv|\phi_j(\widetilde{\mathbf{x}},t=t_n)|^2=|\phi_j^n(\widetilde{\mathbf{x}})|^2$, and it can be integrated exactly as

$$\phi_j(\mathbf{x},t) = \exp\left\{-i\left[P_j(\mathbf{x},t) + \sum_{k=1}^{2}\left(\beta_{jk}|\phi_k^n|^2(t-t_n) + \lambda_{jk}\,\varphi_k(\widetilde{\mathbf{x}},t)\right)\right]\right\}, \tag{3.38}$$

$$\varphi_k(\widetilde{\mathbf{x}},t) = \int_{\mathbb{R}^d}\widetilde{\mathcal{K}}(\widetilde{\mathbf{x}}-\widetilde{\mathbf{y}},t)\,\rho_k(\widetilde{\mathbf{y}},t_n)d\widetilde{\mathbf{y}}, \qquad \widetilde{\mathbf{x}}\in\mathcal{D}, \quad t_n\le t\le t_{n+1}, \tag{3.39}$$

where the time-dependent kernel $\widetilde{\mathcal{K}}(\widetilde{\mathbf{x}},t)$ has the form

$$\widetilde{\mathcal{K}}(\widetilde{\mathbf{x}},t) = \int_{t_n}^{t}\widetilde{U}_{\rm dip}(\widetilde{\mathbf{x}},\tau)d\tau = \begin{cases} -\delta(\widetilde{\mathbf{x}})(t-t_n) - 3\widetilde{L}_3(t)(\frac{1}{4\pi|\widetilde{\mathbf{x}}|}), & \text{3D DDI}, \\ -\frac{3}{2}\widetilde{L}_2(t)(\frac{1}{2\pi|\widetilde{\mathbf{x}}|}), & \text{2D DDI}. \end{cases} \tag{3.40}$$

Here, the differential operators $\widetilde{L}_3(t)=\int_{t_n}^t\partial_{\mathbf{m}(\tau)\mathbf{m}(\tau)}d\tau$ and $\widetilde{L}_2(t)=\int_{t_n}^t\partial_{\mathbf{m}_\perp(\tau)\mathbf{m}_\perp(\tau)}-m_3^2\nabla_\perp^2\,d\tau$ actually can be integrated analytically and have explicit expressions, one can refer to *section 4.1* in [13] for details. The GauSum solver is then applied to evaluate the nonlocal potential $\varphi(\widetilde{\mathbf{x}},t)$ (3.39). In addition,

$$P_j(\widetilde{\mathbf{x}},t) = \int_{t_n}^{t}\mathcal{W}_j(\widetilde{\mathbf{x}},\tau)d\tau. \tag{3.41}$$

Remark 3.2. *If $V_j(\mathbf{x})$ $(j = 1, 2)$ is a harmonic potential as defined in (1.3), i.e. $\mathcal{W}_j$ reads as (3.34), then the integral in (3.41) can be evaluated analytically, i.e.*

$$\int_{t_n}^{t} \mathcal{W}_j(\widetilde{\mathbf{x}}, \tau) d\tau = \frac{w_j^+(\widetilde{x}^2 + \widetilde{y}^2)}{4}(t - t_n) + \frac{w_j^-}{8\Omega}\Big[(\widetilde{x}^2 - \widetilde{y}^2)\big(\sin(2\Omega t) - \sin(2\Omega t_n)\big) \tag{3.42}$$

$$-2\widetilde{x}\widetilde{y}\big(\cos(2\Omega t) - \cos(2\Omega t_n)\big)\Big] + \begin{cases} 0, & d = 2, \\ \frac{1}{2}\gamma_{z,j}^2 \widetilde{z}^2 (t - t_n), & d = 3. \end{cases} \tag{3.43}$$

For a general potential $V_j(\mathbf{x})$, if the integral in (3.41) can not be found analytically, numerical quadratures such as Trapezoidal rule or Simpson's rule can be applied [11, 13].

To simplify the presentation, we will only present the scheme for the 3D case. As for the 2D case, one can modify the algorithm straightforward. Let L, M, N be even positive integers, choose $h_{\widetilde{x}} = \frac{b-a}{L}$, $h_{\widetilde{y}} = \frac{d-c}{M}$ and $h_{\widetilde{z}} = \frac{f-e}{N}$ as the spatial mesh sizes in $\widetilde{x}$-, $\widetilde{y}$-, and $\widetilde{z}$- directions, respectively. Define the index and grid points sets as

$$\begin{aligned} \mathcal{T}_{LMN} &= \{(l, k, m)\,|\, 0 \le l \le L,\ 0 \le k \le M,\ 0 \le m \le N\}, \\ \widetilde{\mathcal{T}}_{LMN} &= \left\{(p, q, r)\,|\, -\frac{L}{2} \le p \le \frac{L}{2} - 1,\ -\frac{M}{2} \le q \le \frac{M}{2} - 1,\ -\frac{N}{2} \le r \le \frac{N}{2} - 1\right\}, \\ \mathcal{G}_{\widetilde{x}\widetilde{y}\widetilde{z}} &= \{(\widetilde{x}_l, \widetilde{y}_k, \widetilde{z}_m) =: (l\, h_{\widetilde{x}} + a,\ k\, h_{\widetilde{y}} + c,\ m\, h_{\widetilde{z}} + e),\ (l, k, m) \in \mathcal{T}_{LMN}\}. \end{aligned}$$

Define the functions

$$W_{pqr}(\widetilde{x}, \widetilde{y}, \widetilde{z}) = e^{i\mu_p^{\widetilde{x}}(\widetilde{x}-a)}\, e^{i\mu_q^{\widetilde{y}}(\widetilde{y}-c)}\, e^{i\mu_r^{\widetilde{z}}(\widetilde{z}-e)}, \quad (p, q, r) \in \widetilde{\mathcal{T}}_{LMN},$$

with

$$\mu_p^{\widetilde{x}} = \frac{2\pi p}{b-a},\ \ \mu_q^{\widetilde{y}} = \frac{2\pi q}{d-c},\ \ \mu_r^{\widetilde{z}} = \frac{2\pi r}{f-e}, \quad (p, q, r) \in \widetilde{\mathcal{T}}_{LMN}.$$

Let $f_{j,lkm}^n$ ($j = 1, 2$, $f_j = \phi_j$, φ_j or P_j) be the numerical approximation of $f_j(\widetilde{x}_l, \widetilde{y}_k, \widetilde{z}_m, t_n)$ for $(l, k, m) \in \mathcal{T}_{LMN}$, $n \ge 0$ and denote $\boldsymbol{\phi}_j^n$ as the solution vector at time $t = t_n$ with components $\big\{\phi_{j,lkm}^n,\ (l, k, m) \in \mathcal{T}_{LMN}\big\}$. Taking the initial data as $\phi_{j,lkm}^0 = \phi_j^0(\widetilde{x}_l, \widetilde{y}_k, \widetilde{z}_m)$ for $(l, k, m) \in \mathcal{T}_{LMN}$, a second-order *Time Splitting Fourier Pseudopectral* (TSFP) method to solve the CGPE (3.29)–(3.30) reads as follows:

$$\phi_{j,lkm}^{(1)} = \sum_{p=-L/2}^{L/2-1} \sum_{q=-M/2}^{M/2-1} \sum_{r=-N/2}^{N/2-1} e^{-\frac{i\Delta t}{4}\left[(\mu_p^{\widetilde{x}})^2 + (\mu_q^{\widetilde{y}})^2 + (\mu_r^{\widetilde{z}})^2\right]} \widehat{(\boldsymbol{\phi}_j^n)}_{pqr}\, W_{pqr}(\widetilde{x}_l, \widetilde{y}_k, \widetilde{z}_m), \tag{3.44}$$

$$\phi_{j,lkm}^{(2)} = \phi_{j,lkm}^{(1)} \exp\left\{-i\left[\Delta t \sum_{s=1,2}\Big(\beta_{js}|\phi_{s,lkm}^{(1)}|^2 + \lambda_{js}\varphi_{s,lkm}^{n+1}\Big) + P_{j,lkm}^{n+1}\right]\right\}, \tag{3.45}$$

$$\phi_{j,lkm}^{n+1} = \sum_{p=-L/2}^{L/2-1} \sum_{q=-M/2}^{M/2-1} \sum_{r=-N/2}^{N/2-1} e^{-\frac{i\Delta t}{4}\left[(\mu_p^{\widetilde{x}})^2 + (\mu_q^{\widetilde{y}})^2 + (\mu_r^{\widetilde{z}})^2\right]} \widehat{(\boldsymbol{\phi}_j^{(2)})}_{pqr}\, W_{pqr}(\widetilde{x}_l, \widetilde{y}_k, \widetilde{z}_m). \tag{3.46}$$

Here, $\widehat{(\boldsymbol{\phi}_j^n)}_{pqr}$ and $\widehat{(\boldsymbol{\phi}_j^{(2)})}_{pqr}$ are the discrete Fourier transform coefficients of the vectors $\boldsymbol{\phi}_j^n$ and $\boldsymbol{\phi}_j^{(2)}$, respectively. We refer this method as TS2-GauSum. This scheme is explicit, efficient, unconditional stable, simple to implement and can be extended to high-order time-splitting schemes easily.

4. Numerical results

In this section, we first test the convergence of the TS2-GauSum method for computing the dynamics of rotating two-component dipolar BEC. Then, we apply our method to investigate some interesting phenomena, such as the dynamics of dipolar BEC with tunable (time-dependent) dipole axis, collapse properties of a dipolar BEC.

4.1. Test of convergence

Here, we first test the spatial and temporal convergence of our method in both 2D and 3D. To demonstrate the results, we first define the following error function

$$e_{\Psi}^{h,\Delta t}(t) =: \|\Psi(\mathbf{x},t_n) - \Psi_{h,\Delta t}^{n}(\mathbf{x})\|_{l^2} = \sqrt{\sum_{j=1}^{2} \|\psi_j(\mathbf{x},t_n) - \psi_{j,h,\Delta t}^{n}(\mathbf{x})\|_{l^2}^2}, \tag{4.47}$$

where $\|\cdot\|_{l^2}$ denotes the discrete l^2 norm, $\psi_{j,h,\Delta t}^{n}$ is the numerical approximation of $\psi_j(\mathbf{x},t_n)$ obtained by the TS2-GauSum method (3.44)-(3.46) with time step Δt and mesh size $h_v = h$ ($v = \widetilde{x}, \widetilde{y}$ in 2D and $v = \widetilde{x}, \widetilde{y}, \widetilde{z}$ in 3D). The dipole axis $\mathbf{n}$ and interaction parameters are chosen as

$$\mathbf{n} = (1,0,0)^T, \qquad \begin{pmatrix} \beta_{11} & \beta_{12} \\ \beta_{21} & \beta_{22} \end{pmatrix} = \beta \begin{pmatrix} 1 & 0.8 \\ 0.8 & 1.2 \end{pmatrix}, \qquad \begin{pmatrix} \lambda_{11} & \lambda_{12} \\ \lambda_{21} & \lambda_{22} \end{pmatrix} = \frac{1}{20} \begin{pmatrix} \beta_{11} & \beta_{12} \\ \beta_{21} & \beta_{22} \end{pmatrix}. \tag{4.48}$$

Moreover, we take the computational domain $\mathcal{D} = [-12,12]^2$ in 2D and $[-8,8]^3$ in 3D and the potential $V_1(\mathbf{x}) = \frac{|\mathbf{x}|^2}{2}$. The potential $V_2(\mathbf{x})$ and initial data $\psi_j^0(\mathbf{x})$ are chosen respectively as

$$V_2(\mathbf{x}) = \begin{cases} (x^2+y^2)/2, \\ (x^2+1.21y^2+z^2)/2, \end{cases} \qquad \psi_j^0(\mathbf{x}) = \begin{cases} \sqrt[4]{\frac{2}{\pi^2}}\, e^{-\frac{(3-j)x^2+jy^2}{2}}, & d=2, \\ \sqrt[4]{\frac{2}{\pi^3}}\, e^{-\frac{(3-j)x^2+jy^2+z^2}{2}}, & d=3, \end{cases} \qquad j=1,2. \tag{4.49}$$

For comparisons, the "exact" solution Ψ is obtained numerically via the TS2-GauSum method on $\mathcal{D}$ with very small mesh size $h = h_0 = \frac{1}{16}$ and time step $\Delta t = \Delta t_0 = 0.0001$. Table 4.1 lists the spatial errors $e_{\Psi}^{h,\Delta t_0}(t)$ and temporal errors $e_{\Psi}^{h_0,\Delta t}(t)$ at time $t = 0.4$ for the 2D CGPE with $\Omega = 0.4$ and different β, while Tab. 4.2 lists those at time $t = 0.1$ for the 3D case with $\Omega = 0.2$ and different β. From Tabs. 4.1-4.2, we can conclude that the TS2-GauSum method is second order (and spectrally) accurate in time (and space).

Table 4.1: Spatial and temporal discretization errors at time $t = 0.4$ for the 2D CGPE with $\Omega = 0.4$ and different β .

$e_{\Psi}^{h,\Delta t_0}$	$h=1$	$h/2$	$h/4$	$h/8$
$\beta=2$	1.0863E-01	2.9827E-03	2.8843E-07	1.0490E-11
$\beta=10$	3.8018E-01	4.2192E-02	7.4791E-05	1.4662E-11
$e_{\Psi}^{h_0,\Delta t}$	$\Delta t=0.01$	$\Delta t/2$	$\Delta t/4$	$\Delta t/8$
$\beta=2$	2.4167E-05	6.0376E-06	1.5075E-06	3.7504E-07
$\beta=10$	2.2051E-04	5.5049E-05	1.3742E-05	3.4187E-06

Table 4.2: Spatial and temporal discretization errors at time $t = 0.1$ for the 3D CGPE with $\Omega = 0.2$ and different β .

$e_{\Psi}^{h,\Delta t_0}$	$h=1$	$h/2$	$h/4$	$h/8$
$\beta=2$	1.51E-02	1.82E-04	1.92E-08	6.60E-13
$\beta=10$	2.60E-02	9.25E-04	8.70E-07	7.25E-13
$e_{\Psi}^{h_0,\Delta t}$	$\Delta t=0.01$	$\Delta t/2$	$\Delta t/4$	$\Delta t/8$
$\beta=2$	6.14E-06	1.53E-06	3.83E-07	9.52E-08
$\beta=10$	7.62E-05	1.90E-05	4.75E-06	1.18E-06

4.2. Dynamics of the center of mass

In this subsection, we study the dynamics of the (scaled) center of mass by directly simulating the CGPE (3.29)-(3.30) via the TS2-GauSum method (3.44)–(3.46). To this end, we take $d = 2$, dipole axis $\mathbf{n} = (1, 0, 0)^T$ and initial data (1.2)

$$\psi_1^0(\mathbf{x}) = \phi(\mathbf{x} - \mathbf{x}_0), \quad \psi_2^0(\mathbf{x}) = \phi(\mathbf{x} + \mathbf{x}_0), \quad \text{with} \quad \phi(\mathbf{x}) = \frac{(x+iy)}{\sqrt{2\pi}} e^{-\frac{x^2+y^2}{2}}, \ \mathbf{x}_0 = (1,1)^T. \tag{4.50}$$

The computational domain, mesh size and time step are respectively taken as $\mathcal{D} = [-16, 16]^2$, $h_{\widetilde{x}} = h_{\widetilde{y}} = \frac{1}{8}$ and $\Delta t = 0.001$. The trapping potentials are chosen as the harmonic ones (1.3) and the following 6 cases are studied ($j = 1, 2$, $k_j = 3 - j$)

- Case 1: $\Omega = 0.5$, $\beta_{11} = \frac{\beta_{22}}{2} = 50$, $\lambda_{jj} = \frac{\beta_{jj}}{10}$, $\beta_{jk_j} = \frac{2\lambda_{jk_j}}{5} = 2$, $\gamma_{x,j} = \gamma_{y,j} = 1$.
- Case 2: $\Omega = 0.5$, $\beta_{jj} = 10\lambda_{jj} = 50$, $\beta_{jk_j} = \frac{2\lambda_{jk_j}}{5} = 2$, $\gamma_{x,1} = \gamma_{y,2} = 1.1$, $\gamma_{y,1} = \gamma_{x,2} = 1$.
- Case 3: $\Omega = 0.5$, $\beta_{jj} = 10\lambda_{jj} = 50$, $\beta_{jk_j} = 2\lambda_{jk_j} = 2$, $\gamma_{x,1} = \gamma_{y,1} = 1$, $\gamma_{x,2} = \gamma_{y,2} = 1.2$.
- Case 4-6: same parameters as in Case 1-3, except only change as $\Omega = 1$, $\Omega = \pi$ and $\Omega = 1$, respectively.

Figures 4.1-4.2 show the dynamics of the (scaled) center of mass $\mathbf{x}_{c,j}(t)$ ($j = 1, 2$) and its trajectory in the Cartesian coordinates for Case 1-6. From Figs. 4.1-4.2 and additional results not shown here for brevity, we can conclude that: (i) When $\Omega < \min\{\gamma_{x,j}, \gamma_{y,j}\}$, then the (scaled) center of mass of the j-th component $\mathbf{x}_{c,j}$ always moves within a bounded domain (cf. Fig. 4.1). Otherwise, it may move helically outward (cf. Fig. 4.2). (ii) If $V_1(\mathbf{x}) = V_2(\mathbf{x})$ with $\gamma_{x,j} = \gamma_{y,j}$, $\beta_{12} = \beta_{21}$ and $\lambda_{12} = \lambda_{21}$, the total center of mass $\mathbf{x}_c$ moves periodically with a period depending on both the rotating frequency and trapping frequency. In addition, the dynamics of $\mathbf{x}_c$ does not depend on the interaction parameters λ_{ij} and β_{ij} ($i, j = 1, 2$), which is consistent with (3.18)-(3.19). (iii) If $\beta_{12} = \beta_{21}$ & $\lambda_{12} = \lambda_{21}$ and each trapping potential is symmetric but $V_1(\mathbf{x}) \neq V_2(\mathbf{x})$, the interaction between two components affects the motion of $\mathbf{x}_{c,j}$ and hence $\mathbf{x}_c$. Actually, the dynamical patterns of the (scaled) center of mass are similar with its single-component counterparts [13], where the center of mass always moves periodically. Nevertheless, due to the interaction between each component, the dynamics patterns are modified and $\mathbf{x}_{c,j}$ moves now quasi-periodically (cf. Fig. 4.1 (c) and 4.2 (f)). (iv) If the trapping potentials are not symmetric, the dynamics of (scaled) center of mass becomes more complicated. Interactions between the two components will affect significantly the dynamics pattern of the center of mass.

4.3. Dynamics of quantized vortex lattices

In the following, we study the dynamics of quantized vortex lattices in the rotating two-component dipolar BECs. To this end, we choose $d = 2$, $\beta_{11} = \beta_{22} = 100, \beta_{12} = \beta_{21} = 70$ and $\Omega = 0.9$. The trapping potentials are chosen as the harmonic ones (1.3) with $\gamma_{x,j} = \gamma_{y,j} = 1, j = 1, 2$. The initial datum (1.2) are chosen as the stationary vortex lattice state computed by the classical gradient-flow method [8, 48] for the chosen parameters without DDI, i.e. $\lambda_{11} = \lambda_{22} = \lambda_{12} = \lambda_{21} = 0$. The dynamics of vortex lattices are studied for the following two cases:

- Case 1: perturb the trapping frequency in component one by setting $\gamma_{x,1} = \gamma_{y,1} = 1.5$.
- Case 2: turn on the dipolar interaction in component one by setting $\mathbf{n} = (1, 0, 0)^T$ and $\lambda_{11} = 10$.

In our simulation, we take $\mathcal{D} = [-12, 12]^2$, $h_{\widetilde{x}} = h_{\widetilde{y}} = \frac{1}{8}$ and $\Delta t = 0.001$. Figure 4.3 shows the contour plots of the density function $|\psi_j(\mathbf{x}, t)|^2$ ($j = 1, 2$) at different times for Case 1 and 2, while Fig. 4.4 shows the dynamics of the angular momentum expectation. From these two figures, we can see that: (i) The total angular momentum expectation is conserved if $\beta_{12} = \beta_{21}$, $\gamma_{x,j} = \gamma_{y,j}$ and $\lambda_{ij} = 0$ ($i, j = 1, 2$), which agrees with (3.4). (ii) If there is no DDI and the trapping potentials are symmetric, the lattices rotate around the

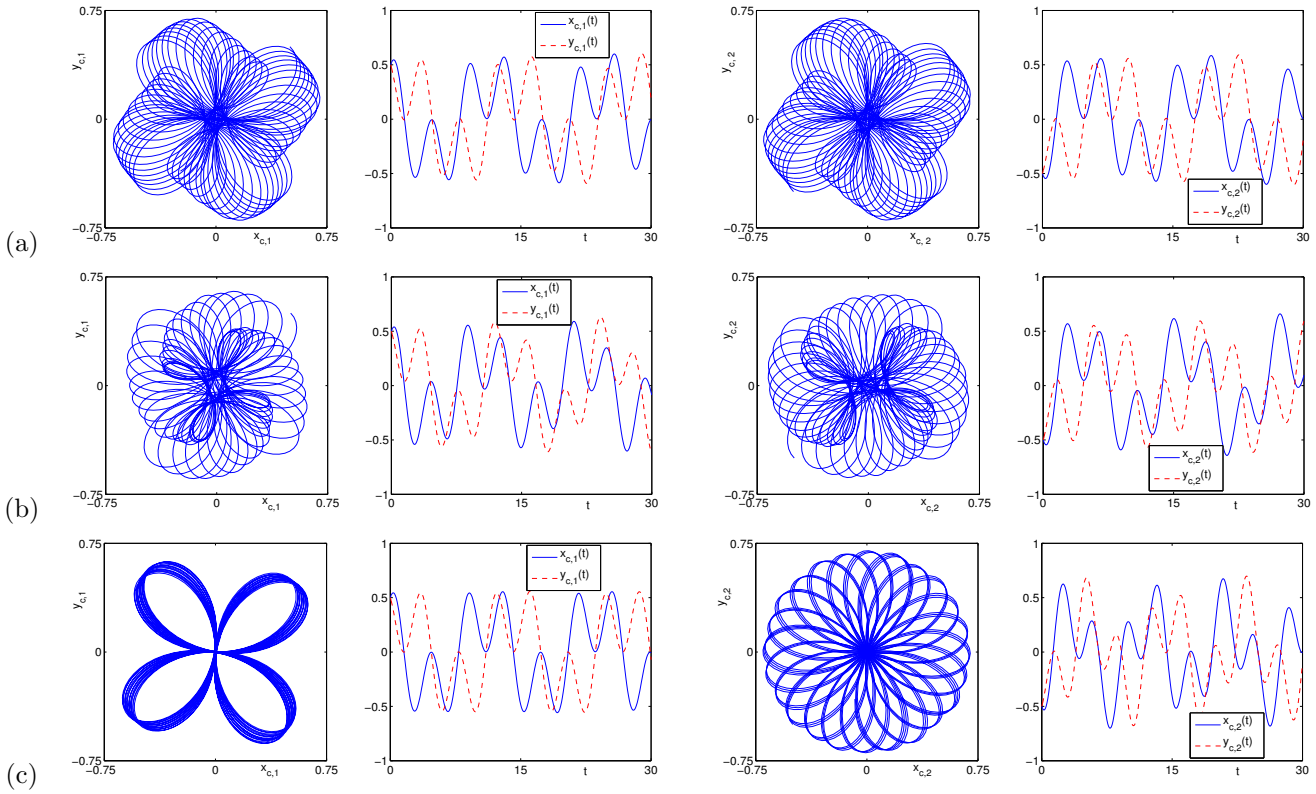

Figure 4.1: The dynamics of (scaled) center of mass and trajectory for $0 \le t \le 200$ for Case 1-3 in Section 4.2: The first two columns for component one and the last two for component two.

origin and keep a similar symmetry and pattern as the initial ones. Meanwhile, the lattices also undergo a breather-like dynamics. (iii) The DDI affects the dynamics very much. Due to the anisotropic nature of DDI, the lattices will rotate to some quite different patterns. The vortices will be redistributed during dynamics. Unlike the single-component BEC, the redistribution here does not seem to be aligned with the dipole axis because of the interaction between the two components. It will be interesting to investigate in further studies how the patterns of vortex lattices re-form and change with respect to the interactions as well as the dipole orientations.

4.4. Numerical results in 3D

In this subsection, we report the dynamics of non-rotating two-component dipolar BECs in different set-ups. To this end, unless stated otherwise, the trapping potential and initial datum are chosen respectively as

$$V_1(\mathbf{x}) = V_2(\mathbf{x}) = \frac{|\mathbf{x}|^2}{2}, \quad \psi_1^0(\mathbf{x}) = \psi_2^0(\mathbf{x}) = \frac{1}{\sqrt{2}}\,\phi_{\rm gs}(\mathbf{x}), \tag{4.51}$$

where $\phi_{\rm gs}(\mathbf{x})$ is the ground state of the single-component non-rotating dipolar BEC with parameters $\mathbf{n} = (0,0,1)^T$, $\beta = 103.58$ and $\lambda = 0.8\,\beta$. Figure 4.5 shows the isosurface of the density for the initial datum $|\psi_j^0(\mathbf{x})|^2 = 0.01$ $(j = 1, 2)$. The computation domain is taken as $\mathcal{D} = [-8, 8]^3$ and the mesh sizes in spatial and temporal direction are chosen as $h_{\widetilde{x}} = h_{\widetilde{y}} = h_{\widetilde{z}} = h = \frac{1}{8}$ and $\Delta t = 0.001$, respectively.

Example 4.1. *Let $\beta_{11} = \beta_{22} = \beta$, $\lambda_{11} = \lambda$ and consider the following three cases: for $j = 1, 2$, $k_j = 3 - j$*

- *Case 1: let $\beta_{jk_j} = 100$ and turn off the DDI in component two, i.e. $\lambda_{22} = \lambda_{jk_j} = 0$. The dipole axis in component one is kept unchanged, i.e. $\mathbf{n} = (0,0,1)^T$.*

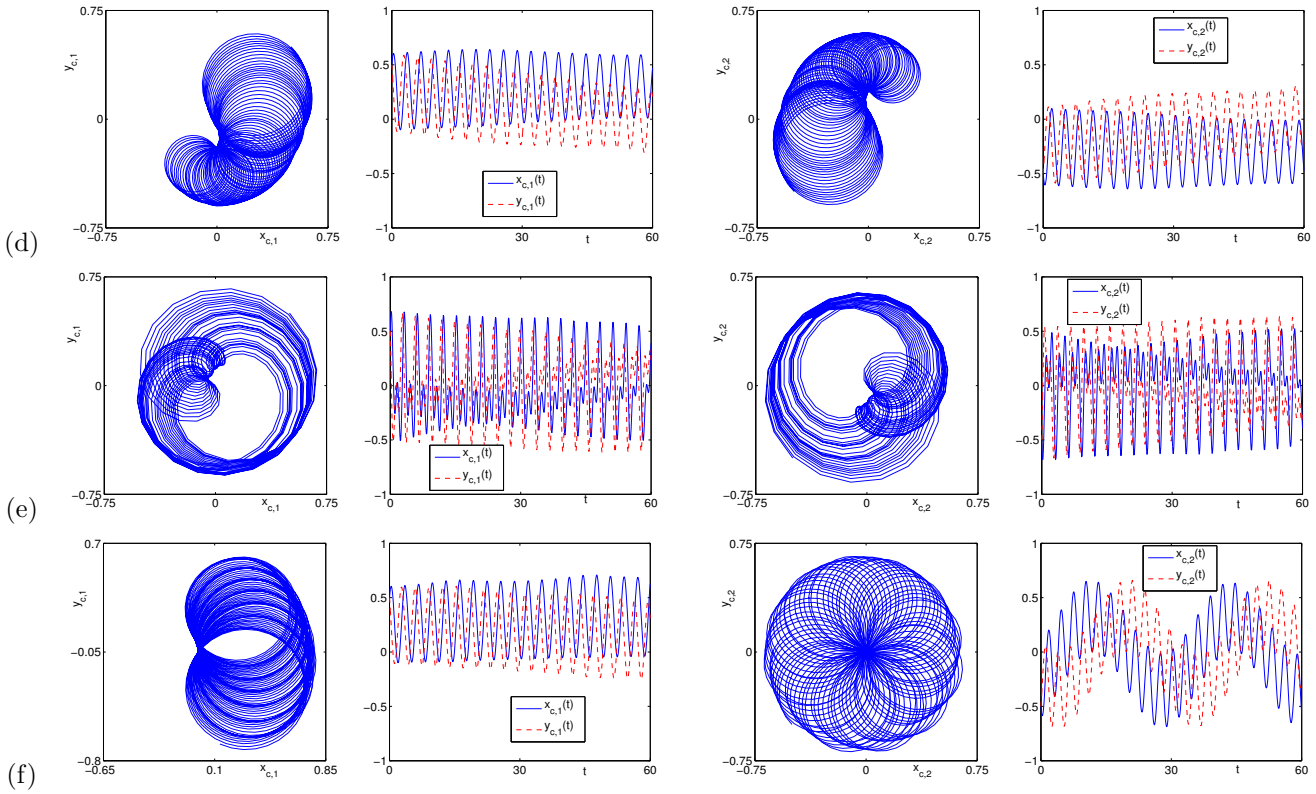

Figure 4.2: The dynamics of (scaled) center of mass and trajectory for $0 \le t \le 150$ for Case 4-6 in Section 4.2: the first two columns for component one and the last two for component two.

- *Case 2 : change the dipole axis to* $\mathbf{n} = (1, 0, 0)^T$ *and keep the other parameters the same as in Case 1.*
- *Case 3: perturb the interatomic interaction as well as the DDI strength, i.e.* $\beta_{12} = \beta_{21} = 50$, $\lambda_{22} = 0.8\beta$ *and* $\lambda_{jk_j} = 0.8\beta_{jk_j}$. *The dipole axis is now time-dependent:* $\mathbf{n} = \big(\sin(t/2), 0, \cos(t/2)\big)^T$.

Figures 4.6-4.8 depict the isosurface of the densities $|\psi_j(\mathbf{x}, t)|^2 = 0.01$ $(j = 1, 2)$ at different times. From these figures and additional results not shown here for brevity, we can see that: (i) The total energy and mass are conserved well. (ii) Phase separation of the two components may come up during dynamics (cf. Figs. 4.6-4.7). In fact, the BECs would undergo mixing and de-mixing formation cyclically [29, 36, 55]. (iii) Similar as those shown in the single-component BEC [14], when the trapping potentials are isotropic, the shapes of the density profile seem unchanged and keep the same symmetric structure with respect to the dipole orientation if the dipole axis rotates slowly (cf. Fig. 4.8).

Example 4.2. *Here we study the collapse dynamics of the dipolar BEC. To this end, we take initial data as (4.51) with same interaction parameters and dipole axis* $\mathbf{n}$ *under trapping potential* $V_1(\mathbf{x}) = V_2(\mathbf{x}) = \frac{x^2+y^2+25z^2}{2}$. *Figure 4.9 shows the isosurface of the densities for the initial datum* $|\psi_j^0(\mathbf{x})|^2 = 0.002$ *(*$j = 1, 2$*). The computational domain and time step are chosen as* $\mathcal{D} = [-8, 8] \times [-8, 8] \times [-4, 4]$ *and* $\Delta t = 0.0001$, *respectively. We consider two cases of collapse dynamics: for* $i, j = 1, 2$, $k_j = 3 - j$

- *Case 1: let* $\beta_{ij} = \beta$ *and change the DDI strength from* $\lambda_{ij} = \lambda$ *to* $\lambda_{11} = \lambda_{jk_j} = 2\lambda_{22} = 10\lambda$.
- *Case 2: let* $\lambda_{jj} = \lambda$, $\lambda_{jk_j} = 0$ *and change* $\beta_{ij} = \beta = 103.58$ *to* $\beta_{ij} = -600$.

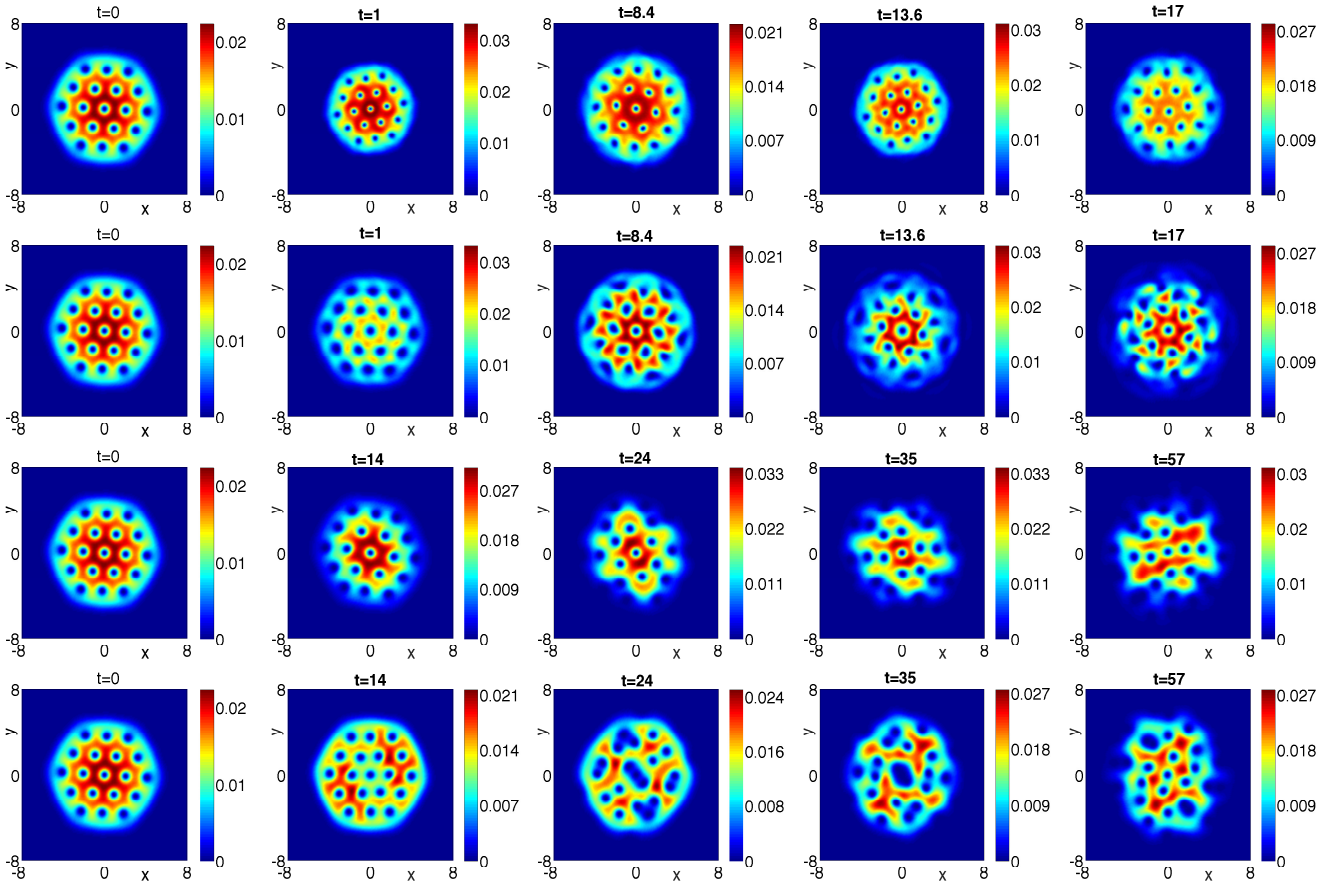

Figure 4.3: Contour plots of the densities $|\psi_1(\mathbf{x},t)|^2$ and $|\psi_2(\mathbf{x},t)|^2$ for Case 1 (top two rows) and Case 2 (bottom) in Section 4.3.

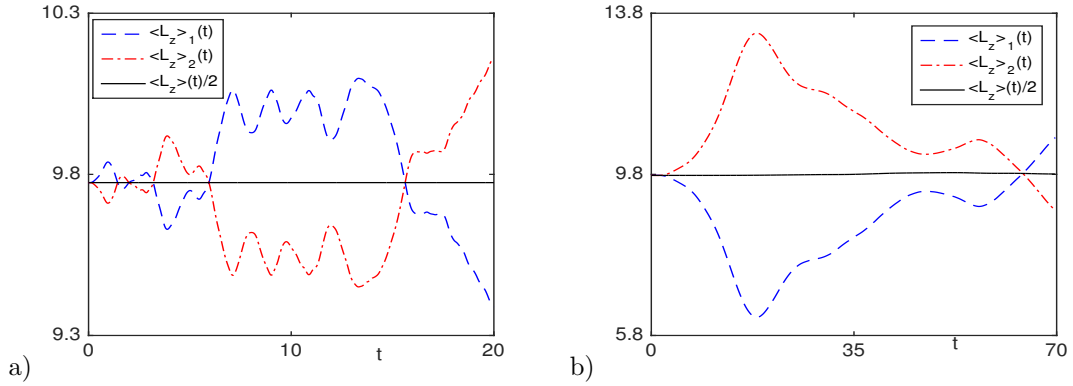

Figure 4.4: Dynamics of the angular momentum expectation for Case 1 (a) and 2 (b) in Section 4.3

Figures 4.10-4.11 depict the isosurface of the densities for $|\psi_j(\mathbf{x},t)|^2 = 0.002$ $(j = 1, 2)$ at different times, while Fig. 4.12 shows the dynamics of energies. From these figures, we can see that: (i) The densities of the dipolar BECs collapse at finite time during the dynamics, i.e. the finite time blow-up of the solution is observed. This is especially clear for Case one where the contact short-range interaction are all repulsive. This reveals clearly the partial-attractive/partial-repulsive property of the DDI. (ii) The total energy and

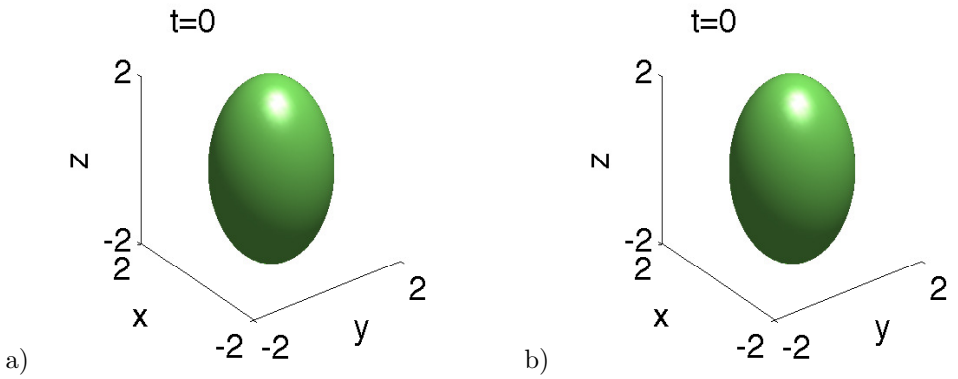

Figure 4.5: Isosurface of the initial densities $\rho_1^0(\mathbf{x}) = |\psi_1^0(\mathbf{x})|^2 = 0.01$ (a) and $\rho_2^0(\mathbf{x}) = |\psi_2^0(\mathbf{x})|^2 = 0.01$ (b) in Example 4.1.

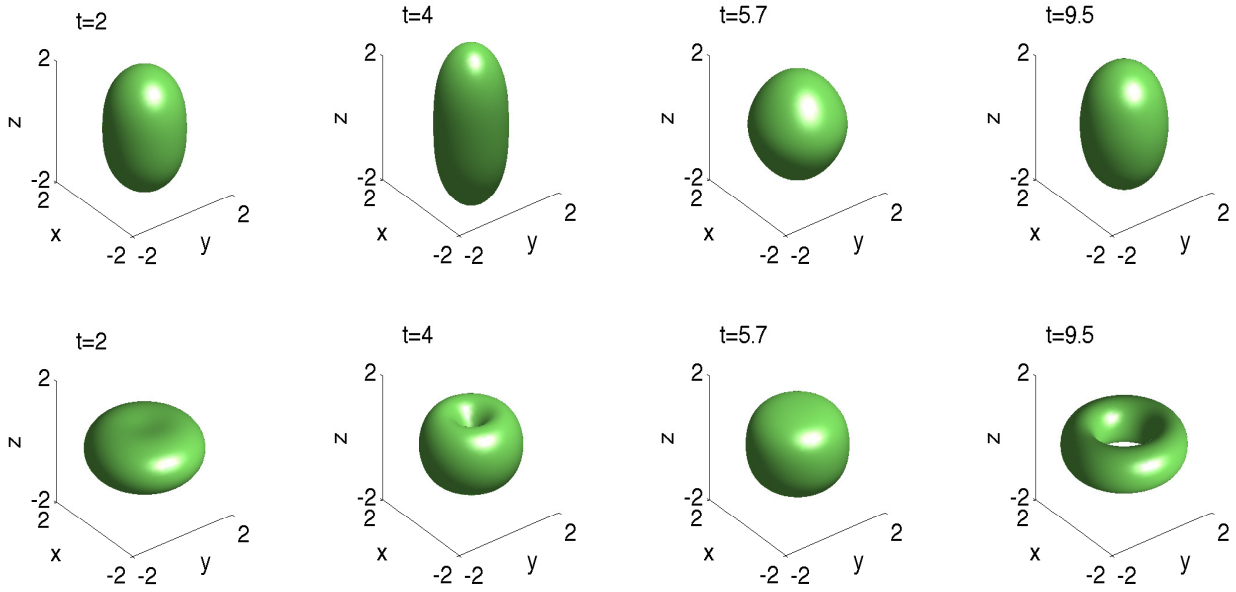

Figure 4.6: Isosurface of the densities $\rho_1(\mathbf{x}, t) = |\psi_1(\mathbf{x}, t)|^2 = 0.01$ (first row) and $\rho_2(\mathbf{x}, t) = |\psi_2(\mathbf{x}, t)|^2 = 0.01$ (second row) at different times in Example 4.1: Case I.

mass are conserved well before the blow-up time. They are not conserved near or after the blow-up time since the solution can no longer be resolved with a fixed mesh size and time steps.

To sum up, Examples 4.1 and 4.2 show that the dynamics of the dipolar BECs are interesting and quite complex. Different structure formations occur during dynamics and they depend heavily on the dipole orientation and the ratio between the DDI and the contact interaction strength. Moreover, the global existence and finite-time blow-up of the solution depend on the interaction parameters, which would be worth an investigation on its own.

5. Conclusions

We propose a robust and accurate numerical scheme to compute the dynamics of rotating two-component dipolar Bose-Einstein condensates (BEC). In rotating Lagrangian coordinates, the original coupled Gross-Pitaevskii equations (CGPE) were reformulated into new equations where the rotating term vanishes. We then developed a new time splitting Fourier pseudospectral method to numerically simulate the dynamics of

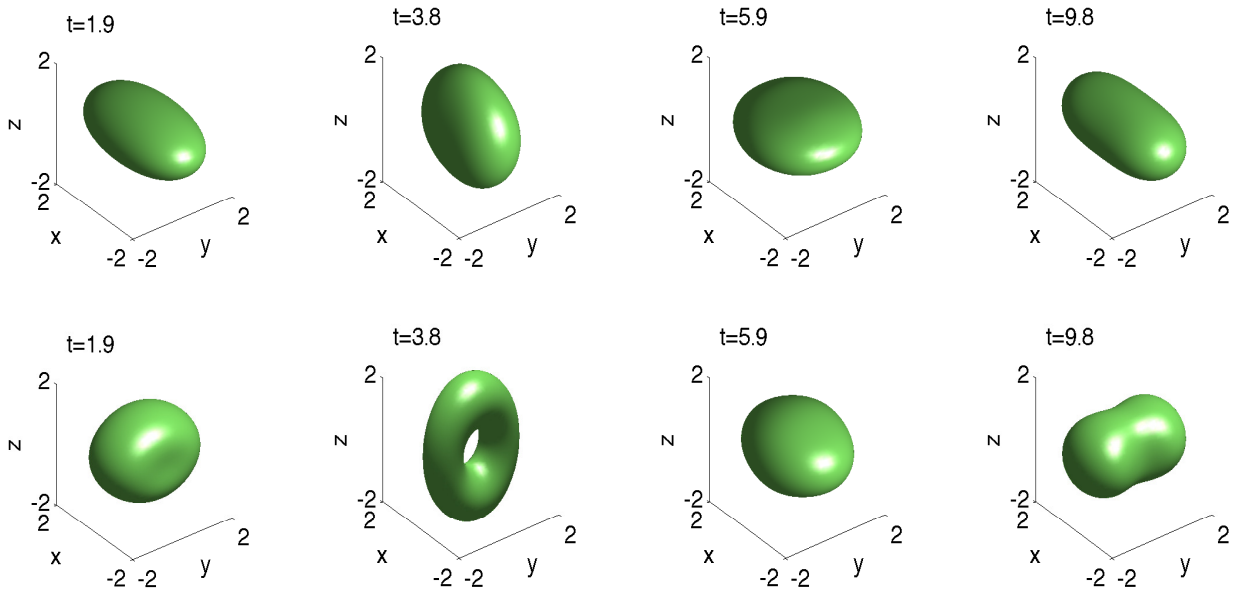

Figure 4.7: Isosurface of the densities $\rho_1(\mathbf{x},t) = |\psi_1(\mathbf{x},t)|^2 = 0.01$ (first row) and $\rho_2(\mathbf{x},t) = |\psi_2(\mathbf{x},t)|^2 = 0.01$ (second row) at different times in Example 4.1: Case II.

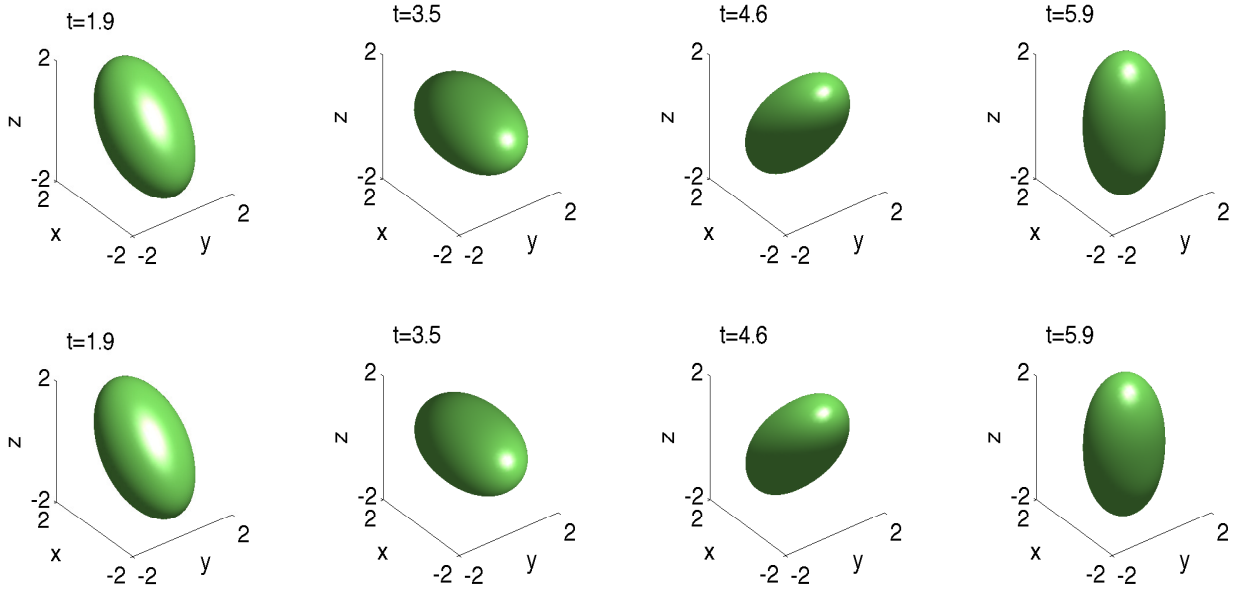

Figure 4.8: Isosurface of the densities $\rho_1(\mathbf{x},t) = |\psi_1(\mathbf{x},t)|^2 = 0.01$ (first row) and $\rho_2(\mathbf{x},t) = |\psi_2(\mathbf{x},t)|^2 = 0.01$ (second row) at different times in Example 4.1: Case III.

the new equations. The nonlocal Dipole-Dipole Interactions (DDI) were evaluated with the Gaussian-sum (GauSum) solver [23], which helps to achieve spectral accuracy within $O(N \log N)$ operations, where N is total number of grid points. Our method is proven to be robust and efficient, and it has spectral accuracy in space and second order accuracy in time. In addition, our numerical schemes can be easily adapted and extended to tackle some more general systems, such as the spin-orbit coupled dipolar BECs [22] and the spinor dipolar BECs [33]. Further, dynamical laws of total mass, energy, center of mass and angular

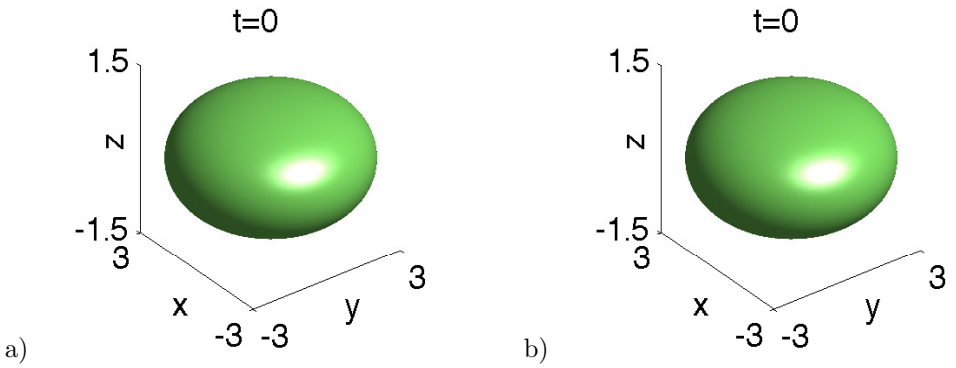

Figure 4.9: Isosurface of the initial densities $\rho_1^0(\mathbf{x}) = |\psi_1^0(\mathbf{x})|^2 = 0.002$ (a) and $\rho_2^0(\mathbf{x}) = |\psi_2^0(\mathbf{x})|^2 = 0.002$ (b) in Example 4.2.

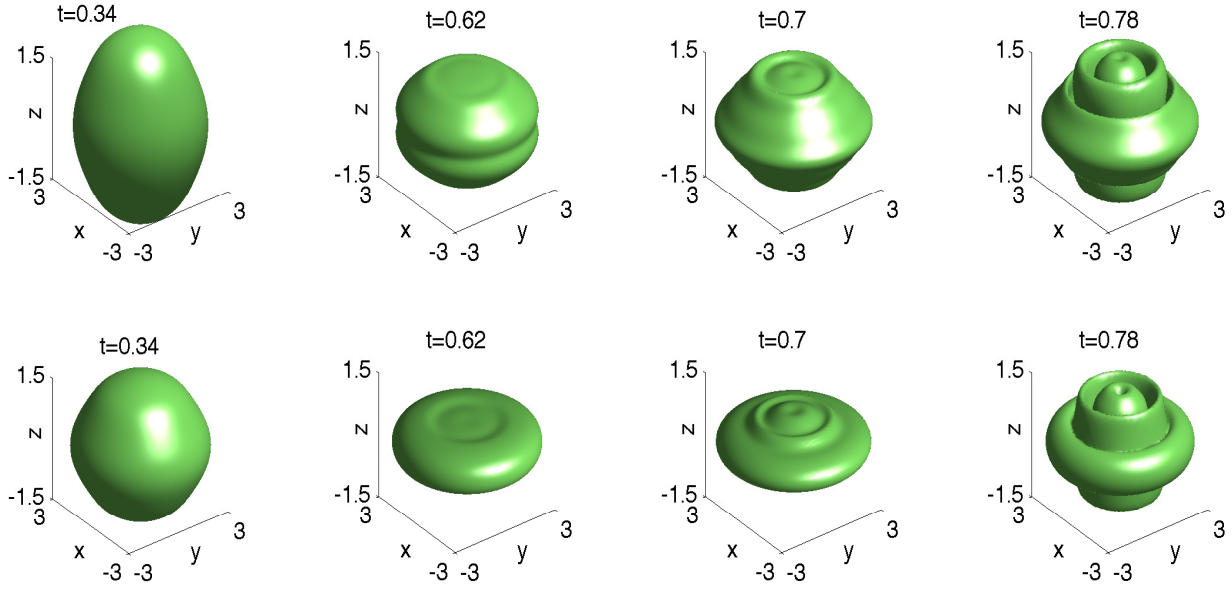

Figure 4.10: Isosurface of the densities $\rho_1(\mathbf{x}, t) = |\psi_1(\mathbf{x}, t)|^2 = 0.002$ (first row) and $\rho_2(\mathbf{x}, t) = |\psi_2(\mathbf{x}, t)|^2 = 0.002$ (second row) at different times for collapse of Case 1 in Example 4.2.

momentum expectation are also derived and confirmed numerically. We then applied the scheme to study the dynamics of quantized vortex lattices, the collapse dynamics of 3D dipolar BECs and identified some phenomena that are peculiar to the rotating two-component dipolar BECs.

Acknowledgements

We acknowledge the support by the French Science Foundation ANR, under grant No ANR-12-MONU-0007-02 ("BECASIM") and grant No ANR-14-CE23-0007-01 "MOONRISE"), by the Austrian Science Foundation FWF under grant No F41 (SFB "VICOM"), grant No F65 (SFB Complexity in PDEs and grant No W1245 (DK "Nonlinear PDEs") and the Schrödinger Fellowship J3784-N32, by the Wiener Wissenschafts- und TechnologieFonds (WWTF) project No MA16-066 (SEQUEX) and by the Natural Science Foundation of China grants No 11261065, No 91430103 and No 11471050. Further, the authors would like to acknowledge the stimulating and helpful discussions with Weizhu Bao. The computation results presented have been achieved in part by using the Vienna Scientific Cluster.

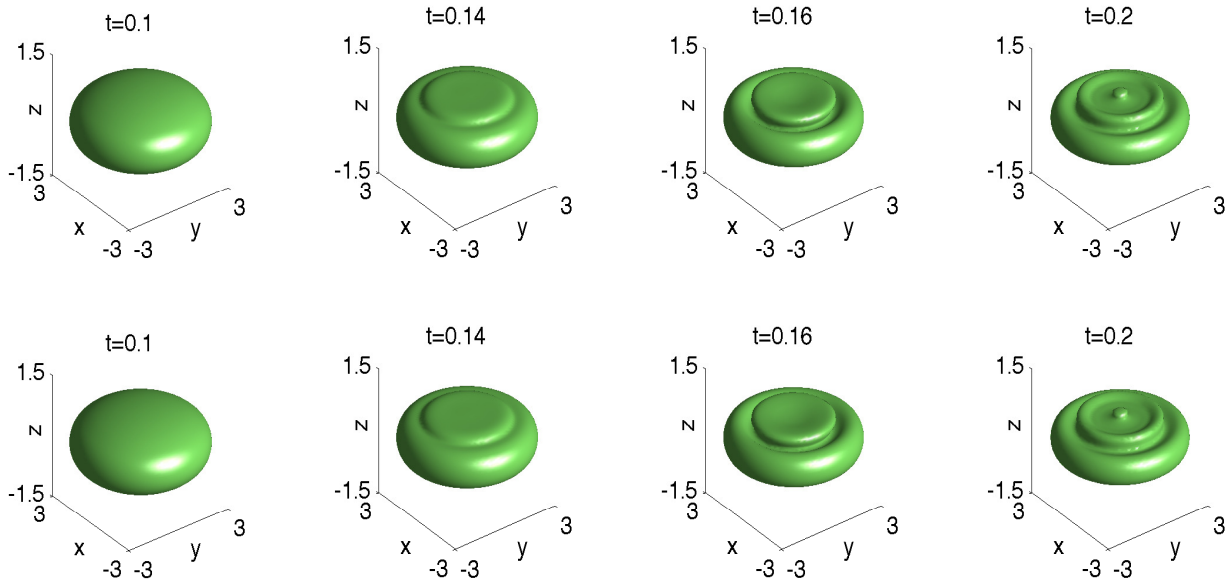

Figure 4.11: Isosurface of the densities $\rho_1(\mathbf{x},t) = |\psi_1(\mathbf{x},t)|^2 = 0.002$ (first row) and $\rho_2(\mathbf{x},t) = |\psi_2(\mathbf{x},t)|^2 = 0.002$ (second row) at different times for collapse of Case 2 in Example 4.2.

(a).

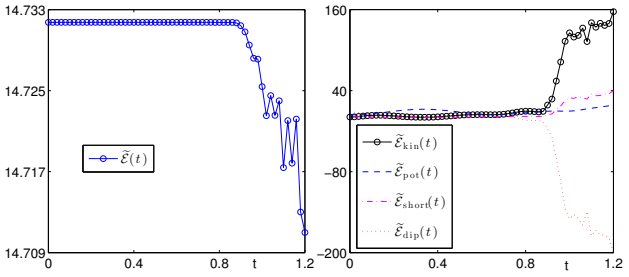

(b).

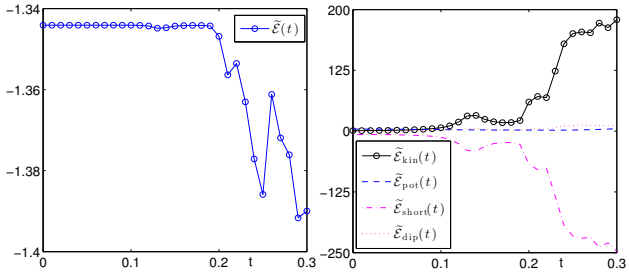

Figure 4.12: Collapse energies for Case 1 (a) and Case 2 (b) in Example 4.2.

References

[1] J. R. Abo-Shaeer, C. Raman, J. M. Vogels and W. Ketterle, *Observation of vortex lattices in Bose-Einstein Condensates*, Science, **292** (2001), pp. 476–479.

[2] S. K. Adhikari and L. E. Young-S, *Statics and dynamics of a binary dipolar Bose–Einstein condensate soliton*, J. Phys. B: At. Mol. Opt. Phys., **47** (2014), article 015302.

[3] M. H. Anderson, J. R. Ensher, M. R. Matthewa, C. E. Wieman and E. A. Cornell, *Observation of Bose-Einstein condensation in a dilute atomic vapor*, Science, **269** (1995), pp. 198–201.

[4] X. Antoine, C. Besse and V. Rispoli, *High-order IMEX-spectral schemes for computing the dynamics of systems of nonlinear Schrödinger/ Gross-Pitaevskii equations*, J. Comput. Phys., **327** (2016), pp. 252–269.

[5] X. Antoine, Q. Tang and Y. Zhang, *On the ground states and dynamics of space fractional nonlinear Schrödinger/Gross-Pitaevskii equations with rotation term and nonlocal nonlinear interactions*, J. Comput. Phys., 325 (2016), pp. 74–97.

[6] K. Aikawa, A. Frisch, M. Mark, S. Baier, A. Rietzler, R. Grimm and F. Ferlaino, *Bose-Einstein condensation of Erbium*, Phys. Rev. Lett., **108** (2012), 210401.

[7] W. Bao, N. Ben Abdallah and Y. Cai, *Gross-Pitaevskii-Poisson equations for dipolar Bose-Einstein condensate with anisotropic confinement*, SIAM J. Math. Anal., **44** (2012), pp. 1713-1741.

[8] W. Bao and Y. Cai, *Ground states of two-component Bose-Einstein Condensates with an internal atomic Josephson junction*, East Asian Journal of Applied Mathematics, **1**(1) (2011), pp. 49-81.

[9] W. Bao and Y. Cai, *Mathematical theory and numerical methods for Bose-Einstein condensation*, Kinet. Relat. Models, **6** (2013), pp. 1-135.

[10] W. Bao, Y. Cai and H. Wang, *Efficient numerical methods for computing ground states and dynamics of dipolar Bose-Einstein condensates*, J. Comput. Phys., **229** (2010), pp. 7874–7892.
[11] W. Bao, Q. Du and Y. Zhang, *Dynamics of rotating Bose–Einstein condensates and its efficient and accurate numerical computation*, SIAM J. Appl. Math., **66** (2006), pp. 758–786.
[12] W. Bao, S. Jiang, Q. Tang and Y. Zhang, *Computing the ground state and dynamics of the nonlinear Schrödinger equation with nonlocal interactions via the nonuniform FFT*, J. Comput. Phys., **296** (2015), pp. 72–89.
[13] W. Bao, D. Marahrens, Q. Tang and Y. Zhang, *A simple and efficient numerical method for computing dynamics of rotating dipolar Bose–Einstein condensation via a rotating Lagrange coordinate*, SIAM J. Sci. Comput., **35** (2013), pp. A2671–A2695.
[14] W. Bao, Q. Tang and Y. Zhang, *Accurate and efficient numerical methods for computing ground states and dynamics of dipolar Bose-Einstein condensates via the nonuniform FFT*, Commun. Comput. Phys., **19**(5) (2016), pp. 1141–1166.
[15] M. A. Baranov, *Theoretical progress in many body physics of dipolar gases*, Phys. Rep., **464** (2008), pp. 71–111.
[16] C. Besse, G. Dujardin and I. L. Violet, *High order exponential integrators for nonlinear Schödinger equations with application to rotating Bose–Einstein condensates*, (2015), hal-01170888.
[17] C. C. Bradley, C. A. Sackett, J. J. Tollett and R. G. Hulet, *Evidence of Bose-Einstein condensation in an atomic gas with attractive interaction*, Phys. Rev. Lett., **75** (1995), pp. 1687–1690.
[18] Y. Cai, M. Rosenkranz, Z. Lei and W. Bao, *Mean-field regime of trapped dipolar Bose-Einstein condensates in one and two dimensions*, Phys. Rev. A, **82** (2010), article 043623.
[19] R. Carles, P. A. Markowich and C. Sparber, *On the Gross-Pitaevskii equation for trapped dipolar quantum gases*, Nonlinearity, **21** (2008), pp. 2569–2590.
[20] N. R. Cooper, E. H. Rezayi and S. H. Simon, *Vortex lattices in rotating atomic Bose gases with dipolar interactions*, Phys. Rev. Lett., **95** (2005), article 200402.
[21] K. B. Davis, M. O. Mewes, M. R. Andrews, N. J. van Druten, D. S. Durfee, D. M. Kurn and W. Ketterle, *Bose-Einstein condensation in a gas of sodium atoms*, Phys. Rev. Lett., **75** (1995), pp. 3969–3973.
[22] Y. Deng, J. Cheng, H. Jing, C.-P. Sun and S. Yi, *Spin-orbit coupled dipolar Bose-Einstein condensates*, Phys. Rev. Lett., **108** (2012), article 125301.
[23] L. Exl, N.J. Mauser and Y. Zhang, *Accurate and efficient computation of nonlocal potentials based on Gaussian-sum approximation*, arXiv:1501.04438.
[24] M. Fattori, G. Roati, B. Deissler, C. D'errico, M. Zaccanti, M. Jona-Lasinio, L. Santos, M. Inguscio and G. Modugno, *Magnetic dipolar interaction in a Bose-Einstein condensate atomic interferometer*, Phys. Rev. Lett., **101** (2008), article 190405.
[25] A. L. Fetter, *Rotating trapped Bose-Einstein condensates*, Rev. Mod. Phys., **81** (2009), pp. 647–691.
[26] N. Ghazanfari, A. Keles, and M. Ö. Oktel, *Vortex lattices in dipolar two component Bose–Einstein condensates*, Phys. Rev. A., **89**, article 025601.
[27] G. Gligoric, A. Maluckov, M. Stepic, L. Hadzievski and B. Malomed, *Transition to miscibility in linearly coupled binary dipolar Bose-Einstein condensates*, Phys. Rev. A, **82** (2010), article 033624.
[28] A. Griesmaier, J. Werner, S. Hensler, J. Stuhler and T. Pfau, *Bose–Einstein condensation of Chromium*, Phys. Rev. Lett., **94** (2005), article 160401.
[29] D. S. Hall, M. R. Matthews, J. R. Ensher, C. E. Wieman and E. A. Cornell, *Dynamics of component separation in a binary mixture of Bose–Einstein condensates*, Phys. Rev. Lett., **81** (1998), 1539–1542.
[30] Z. Huang, P. A. Markowich and C. Sparber, *Numerical simulation of trapped dipolar quantum gases: collapse studies and vortex dynamics*, Kinetic and Related Models, **3** (2010), pp. 181–194.
[31] D. M. Jezek, P. Capuzzia and H. M. Cataldo, *Structure of vortices in two-component Bose-Einstein condensates*, Phys. Rev. A, **64** (2001), article 023605.
[32] S. Jiang, L. Greengard and W. Bao, *Fast and accurate evaluation of dipolar interaction in Bose-Einstein condensates*, SIAM J. Sci. Comput., **36** (2014), pp. B777–B794.
[33] Y. Kawaguchi and M. Ueda, Spinor Bose-Einstein condensates, Phys. Rep., **520** (2012), 253–381.
[34] K. Kasamatsu, M. Tsubota and M. Ueda, *Vortex phase diagram in rotating two component Bose–Einstein condensate*, Phys. Rev. Lett., **91** (2003), article 150406.
[35] S. Komineas and N. R. Cooper, *Vortex lattices in Bose-Einstein condensates with dipolar interactions beyond the weak-interaction limit*, Phys. Rev. A., **75** (2007), article 023623.
[36] T. Lahaye, C. Menotti, L. Santos, M. Lewenstein and T. Pfau, *The physics of dipolar bosonic quantum gases*, Rep. Prog. Phys., **72** (2009), article 126401.
[37] T. Lahaye, J. Metz, B. Fröhlich, T. Koch, M. Meister, A. Griesmaier, T. Pfau, H. Saito, Y. Kawaguchi and M. Ueda, *D-wave collapse and explosion of a dipolar Bose-Einstein condensate*, Phys. Rev. Lett., **101** (2008), article 080401.
[38] S. Li, X. Li and D. Hua, *The numerical method for computing the ground state of the two-component dipolar Bose-Einstein condensate*, Advances in Difference Equations, **204** (2013).
[39] M. Lu, N. Q. Burdick, S. H. Youn and B. L. Lev, *Strongly dipolar Bose–Einstein condensate of Dysprosium*, Phys. Rev. Lett., **107** (2011), article 190401.
[40] K. W. Madison, F. Chevy, W. Wohlleben and J. Dalibard, *Vortex formation in a stirred Bose-Einstein condensate*, Phys. Rev. Lett., **84** (2000), 806–809.
[41] J. Ming, Q. Tang and Y. Zhang, *An efficient spectral method for computing dynamics of rotating two-component Bose-Einstein condensates via coordinate transformation*, J. Comput. Phys., **258** (2014), pp. 538–554.
[42] N. G. Parker, C. Ticknor, A. M. Martin and D. H. J. O'Dell, *Structure formation during the collapse of a dipolar*

atomic Bose-Einstein condensate, Phys. Rev. A, **79** (2009), article 013617.
[43] L. P. Pitaevskii and S. Stringari, *"Bose-Einstein Condensation"*, Clarendon Press, Oxford, 2003.
[44] H. Saito, Y. Kawaguchi and M. Ueda, *Ferrofluidity in a two component dipolar Bose–Einstein condensation*, Phys. Rev. Lett., **102** (2009), article 230403.
[45] L. Santos, G. Shlyapnikov, P. Zoller and M. Lewenstein, *Bose-Einstein condensation in trapped dipolar gases*, Phys. Rev. Lett., **85** (2000), pp. 1791–1797.
[46] J. M. Sage, S. Sainis, T. Bergeman and D. DeMille, *Optical production of ultracold polar molecules*, Phys. Rev. Lett., **94** (2005), article 203001.
[47] Q. Tang, *Numerical Studies on Quantized Vortex Dynamics in Superfluidity and Superconductivity*, Ph.D. thesis, National University of Singapore, 2013.
[48] H. Wang, *Numerical Simulations on Stationary States for Rotating Two-Component Bose-Einstein Condensates*, J Sci. Comput., **38** (2009), pp. 149–163.
[49] H. Wang, *Quantized Vortex States and Dynamics in Bose-Einstein Condensates*, Ph.D. thesis, National University of Singapore, 2006.
[50] H. Wang, *A time-splitting spectral method for coupled Gross–Pitaevskii equations with applications to rotating Bose–Einstein condensates*, J. Comput. Appl. Math., **205** (2007), pp. 88–104.
[51] L. Wang, B. Dong, G. Chen, W. Han, S. Zhang, Y. Shi and X. Zhang, *Vortices of a rotating two component dipolar Bose–Einstein condensate in an optical lattice*, Phys. Lett. A, **380** (2016), 435–438.
[52] K. Xi, J. Li and D. Shi, *Phase separation of a two component dipolar Bose–Einstein condensate in the quasi-one dimensional and quasi-two dimensional regime*, Phys. Rev. A, **84** (2011), article 013619.
[53] S. Yi and L. You, *Trapped atomic condensates with anisotropic interactions*, Phys. Rev. A, **61** (2000), article 041604(R).
[54] S. Yi and L. You, *Trapped condensates of atoms with dipole interactions*, Phys. Rev. A, **63** (2001), article 053607.
[55] L. E. Young-S. and S. K. Adhikari, *Mixing, demixing and structure formation in a binary dipolar Bose–Einstein condensate*, Phys. Rev. A, **86** (2012), article 063611.
[56] X. Zhang, L. Wen, C. Dai, R. Dong, H. Jiang, H. Chang and S. Zhang, *Exotic vortex lattices in a rotating binary dipolar Bose–Einstein condensate*, Sci. Rep., **6** (2016), article 19380.
[57] J. Zhang and H. Zhai, *Vortex lattices in planar Bose–Einstein condensates with dipolar interactions*, Phys. Rev. Lett., **95** (2005), article 200403.
[58] Y. Zhang, W. Bao and H. Li, *Dynamics of rotating two-component Bose–Einstein condensates and its efficient computation*, Physica D, **234** (2007), pp. 49–69.
[59] Y. Zhao, J. An and C. Gong, *Vortex competition in a rotating two component dipolar Bose–Einstein condensate*, Phys. Rev. A, **87** (2013), article 013605.